Reconnaissance, Signal Stabilization using Deterministic/Gaussian Signals, & Suppression of Limit Cycles in 3×3 Systems with Memory Type Nonlinearities

KARTIK CHANDRA PATRA[a*], ASUTOSH PATNAIK
Department of Electrical Engineering
C. V. Raman Global University, Bhubaneswar,
Odisha 752054,
INDIA
[a]ORCID ID: 0000-0002-4693-4883

*Corresponding Author:

Abstract: - The paper presents an innovative graphical technique that uses computer graphics in conjunction with geometric tools in the estimation of limit cycles (LC) in 3×3 nonlinear (NL) systems with rectangular hysteresis and backlash Nonlinearities. In the event the system exhibits LCs under autonomous conditions, the work explores the possibility of mitigating/quenching limit cycling oscillations through signal stabilization using high-frequency deterministic/Gaussian signals. In addition, another attempt is taken to suppress LCs by the pole placement (PP) technique through state feedback. The state feedback gain matrix K is determined either by arbitrary selection ensuring a complete state controllability condition or by optimal selection from the Riccati equation. To avoid the mathematical complexity of formulation for 3×3 memory-type Nonlinearities, in particular for estimation/prediction of LCs, a novel graphical method is developed using the most common and popular describing function (DF), assuming harmonic balance with proper justification that the linear components of systems possess low-pass characteristics. The complexity and criticality in the mathematical expression (which diminish problem insight) are mitigated when the system exhibits LC predominantly at a single frequency. The proposed methods are demonstrated through practical examples and validated using digital simulations, implemented via a program developed in MATLAB. These results are further substantiated by those obtained using the SIMULINK toolbox in the MATLAB environment.

Key-Words: - Describing function; Limit cycles; Signal Stabilization; Pole Placement

Received: March 15, 2026. Revised: May 18, 2026. Accepted: June 11, 2026. Published: July 13, 2026.

1 Introduction

Researchers have been focusing on prediction LCs in 2×2 NL systems for several decades [1-40]. In fact, the issue is more significant and severe in the case of memory-type nonlinearities. In [41-43] where it has been addressed a little. It was surprising that till [5], practically no literature was available that addresses the mitigating/quenching of such LCs. In [38], the researchers have discussed the quenching of LC in memory-type Nonlinearities and elaborated the concept of synchronization and desynchronization (using incremental describing function (IDF)). They illustrated these phenomena through examples in 2×2 NL systems lucidly. However, literature scarcely available addresses 3×3 NL systems. In [30], it has been stated that the boiler turbine unit is a 3×3 system that demonstrates NL dynamics over a wide range of operating conditions. Some chemical processes are inherently multi-dimensional in nature. These processes can often be represented by a 3×3 model. Limit cycles (LCs) have been observed in such systems. In [31, 32, 42, 44], the researchers have confined their research to non-memory-type Nonlinearities in the 3-dimensional case. The describing function (DF) technique is absolutely/totally suitable for prediction of limit cycles [4, 5, 10, 11, 13, 20, 45]. Prediction/estimation of LC in 3×3 NL systems well-suited with the configuration of general 3×3 systems in [46] draws attention and is thus presented in this work. Analytically dealing with this problem using mathematical formulation, following the above structure particularly for memory-type Nonlinearities, is extremely complex and involved and critical (which loses insight into the problem, even with the assumption of harmonic linearization/balance [40]). It is always justified since the linear parts of the system possesses low-pass characteristics. To make the problem still less complex and simple, it is assumed the exhibition of LC is predominantly at a single frequency, particularly for multidimensional cases. Under these circumstances the graphical method has been developed for prediction/estimation of LCs in 3×3 memory type NL systems. The graphical approach provides an explicit and novel insight into the problem. The backlash is a very common and, in some cases, inherent characteristic in physical systems, which causes any third or higher-order system to exhibit LCs. The existence or exhibition of limit cycles (LCs) acts as a constraint on control performance. In the robotics and automation industry, it adversely affects speed and position control. This issue has been addressed in multivariable systems [26, 27, 31, 34, 40]. Another notable adverse effect of LC due to the inherent backlash characteristics of speed governors hampers the performance in load frequency control (LFC) [31, 43].

The present work is proposed in sequences as given below. Immediately after the Notation Table, section 1 introduces the subject as given in the Introduction. Section 2 introduces a graphical method for the estimation and prediction of LC in 3×3 systems exhibiting memory-type nonlinearities. The procedure has been illustrated through Example 1 (Rectangular Hysteresis) and Example 2 (Backlash-type nonlinearities). These may be considered as extensions/advancements presented in [38, 40, 46].

Section 3 narrates the process of signal stabilization and illustrates it through memory-type nonlinearities (rectangular hysteresis and backlash) by deterministic/Gaussian signals. In Section 4, LC suppression is achieved via a pole-placement approach using a state feedback gain matrix K. This matrix is obtained either by arbitrary selection, subject to complete state controllability [49], or by optimal design based on the Riccati equation [50].

Analysis of system 3×3 dynamics NL system has been presented in section 3 as shown in Fig. 1. Under autonomous conditions (U = 0), the governing equations for determining the LC expression in the frequency domain are given by X = –HC and C = GN(X)X. Combining these relations yields X = –HGNX = AX, where A = –HGN, as presented in [40], which facilitates eigenvalue computation as described in Section 2.1 of [44]. Xi denotes the amplitude of the input sinusoidal signal, and Ci represents the amplitude of the corresponding output signal.

2 Analysis of Limit Cycles in 3×3 Systems Subject to Memory-Based Nonlinearities and Their Dynamic Characteristics

2.1 Graphical Method

Due to the high level of complexity and the extensive analytical computations involved, a graphical method [44, 46] has been adopted to investigate LC in 3×3 nonlinear systems. The analysis focuses on simplifying the investigation of system behavior using this approach. A system composed of three interconnected subsystems is considered, as depicted in Fig. 1. In this configuration, N1, N2, and N3 represent three nonlinear elements, each exhibiting rectangular hysteresis-type input–output characteristics. These characteristics are shown in Fig. 2(a), 2(b), and 2(c), respectively. The elements G1(s), G2(s), and G3(s) denote the transfer functions of the three linear components within the system.

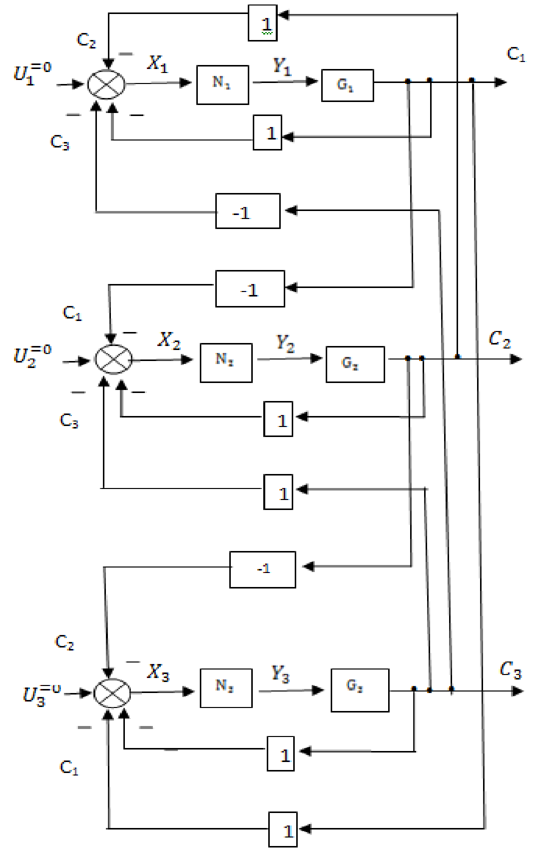

Fig. 1: A group of multivariable NL systems with a 3×3 structure

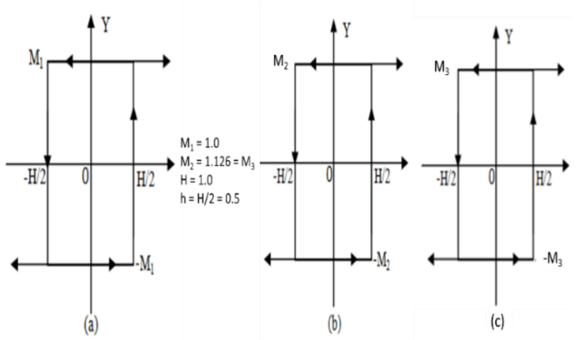

Fig. 2: Rectangular hysteresis behaviour observed in the NL components N_1, N_2 and N_3

A graphical approach based on a normalized phasor diagram, as discussed in [40], is employed for the analysis of 3×3 multivariable systems for the investigation of LC. The approach is demonstrated through Examples 1 and 2. The analysis is carried out under the assumption that the system exhibits self-sustained oscillations. These oscillations are assumed to occur predominantly at a single frequency.

The presence of rectangular hysteresis Nonlinearities introduces additional phase contributions to the overall loop phase. These contributions combine with the phase angles generated by the linear subsystems G_1 (jω), G_2 (jω) and G_3 (jω), corresponding to subsystems S_1, S_2 and S_3 respectively. The existence of LC is governed by three necessary conditions [46]:

1. Phase Condition

For memory-type Nonlinearities, the total loop phase must satisfy:

$$\theta = 180^o = \angle N_1 + \angle N_2 + \angle N_3 + \angle G_1 + \angle G_2 + \angle G_3$$

Where $\angle G_i$ represents the phase of the linear elements and $\angle N_i$ denotes the phase contribution of the NL elements through their describing functions.

2. Gain Condition

The loop gain must satisfy:

$$\frac{C_1}{R_1} \times \frac{C_2}{R_2} \times \frac{C_3}{R_3} = 1$$

where,

$$\frac{C_1}{R_1} = \frac{G_1(j\omega)N_1(X_{m1},\omega)}{1 + G_1(j\omega)N_1(X_{m1},\omega)}$$

$$\frac{C_2}{R_2} = \frac{G_2(j\omega)N_2(X_{m2},\omega)}{1 + G_2(j\omega)N_2(X_{m2},\omega)}$$

$$\frac{C_3}{R_3} = \frac{G_3(j\omega)N_3(X_{m3},\omega)}{1 + G_3(j\omega)N_3(X_{m3},\omega)}$$

3. Amplitude Ratio Condition

The amplitude relationships among the system variables must satisfy:

$$\frac{X_1}{X_2} = \frac{V_1}{V_2}, \qquad \frac{X_2}{X_3} = \frac{V_2}{V_3}, \qquad \frac{X_3}{X_1} = \frac{V_3}{V_1}$$

where

$X_1 = X_{m1},\ X_2 = X_{m2},\ X_3 = X_{m3}$

The quantities $V_1, V_2,$ and V_3 are the eigenvectors corresponding to the eigenvalues $\lambda_1, \lambda_2,$ and λ_3 of the system matrix A, respectively.

2.1.1 For the Example 1

Let the system be considered as illustrated in Fig. 2 featuring:

$$G_1(s) = \frac{2.0}{s(s+1.0)^2}$$
$$G_2(s) = \frac{1.0}{s(s+4.0)}$$
$$G_2(s) = \frac{1.0}{s(s+2.0)}$$

and the nonlinear (NL) elements exhibit rectangular hysteresis (RH) characteristics with parameters M_1 = 1.0, M_2 = 1.126, and M_3 = 1.126. The corresponding values are H = 1.0 and h = H/2 = 0.5, as shown in Fig. 3(a), Fig. 3(b), and Fig. 3(c). The DF for a RH nonlinearity is expressed as:

N (X_m, ω) = $\left|\frac{Y}{X_m} < \phi\right|$ = 0 , X< $\frac{H}{2}$ …(1)

$\frac{4M}{\phi X} <$ - $\sin^{-1}\frac{H}{2X}$, X> $\frac{H}{2}$

This expression can be expanded in the (a + jb) form. This is consistent with Eqs. (2), (4), and (6).

$$N_1(X_1,\omega_1) = \frac{4M_1}{\pi X_1}\left[\cos\left(sin^{-1}\frac{1}{2X_1}\right) - j\frac{1}{2X_1}\right] \ldots (2)$$

$$N_1{'}(X_1,\omega_1) = \frac{-4M_1}{\pi X_1^2}\cos\left(sin^{-1}\frac{1}{2X_1}\right) + \frac{2}{\pi X_1^4} \times \frac{1}{\sqrt{1-(^1/_{4X_1})}} + j\frac{4M_1}{\pi X_1^3} \ldots (3)$$

$$N_2(X_2,\omega_2) = \frac{4M_2}{\pi X_2}\left[\cos\left(sin^{-1}\frac{1}{2X_2}\right) - j\frac{1}{2X_2}\right] \ldots (4)$$

$$N_2{'}(X_2,\omega_2) = \frac{-4M_2}{\pi X_2^2}\cos\left(sin^{-1}\frac{1}{2X_2}\right) + \frac{2}{\pi X_2^4} \times \frac{1}{\sqrt{1-(^1/_{4X_2})}} + j\frac{4M_2}{\pi X_2^3} \ldots (5)$$

$$N_3(X_3,\omega_3) = \frac{4M_3}{\pi X_3}\left[\cos\left(sin^{-1}\frac{1}{2X_3}\right) - j\frac{1}{2X_3}\right] \ldots (6)$$

$$N_3{}'(X_3,\omega_3) = \frac{-4M_3}{\pi X_3^2}\cos\left(sin^{-1}\frac{1}{2X_3}\right) + \frac{2}{\pi X_3^4} \times \frac{1}{\sqrt{1-({}^{1}/_{4X_3})}} + j\frac{4M_3}{\pi X_3^3} \quad \ldots (7)$$

The Newton–Raphson (NR) method was applied to solve Equations (2), (4), and (6). During the iterative computations, the phase angles were not explicitly incorporated. Instead, they were introduced later in the loop angle evaluations. This is shown in Equations (8) to (10). On the other hand, the phase angle constraint is also considered, as indicated in Eqn. (i):

$$\theta = 180^o = \angle N_1 + \angle N_2 + \angle N_3 + \angle G_1 + \angle G_2 + \angle G_3$$

was evaluated at each iteration.

Normalized phase diagrams (NPD) were developed for three distinct configurations. In Set 1, subsystems S_1, S_2, and S_3 are considered with C_1 (−), C_2 (−), and C_3 (+), as shown in Fig. 3(a). In Set 2, the arrangement is S_2, S_3, and S_1 with C_2 (−), C_3 (−), and C_1 (+), as illustrated in Fig. 3(b). In Set 3, subsystems S_1, S_3, and S_2 are analyzed with C_3 (−), C_1 (−), and C_2 (+), as shown in Fig. 3(c).

For set 1: $\theta_{L_1} = \theta_{N_1(X_1,\omega)} + \theta_{G_1(j\omega)}$

$$\theta_{L_1} = -\sin^{-1}\frac{H}{2X_1} - \frac{\pi}{2} - 2\tan^{-1}\omega \quad \ldots (8)$$

For set 2: $\theta_{L_2} = \theta_{N_2(X_2,\omega)} + \theta_{G_2(j\omega)}$

or$\theta_{L_2} = -\sin^{-1}\frac{H}{2X_2} - \frac{\pi}{2} - \tan^{-1}\frac{\omega}{4}$ ... (9)

For set 3: $\theta_{L_3} = \theta_{N_3(X_3,\omega)} + \theta_{G_3(j\omega)}$

or $\theta_{L_3} = -\sin^{-1}\frac{H}{2X_3} - \frac{\pi}{2} - \tan^{-1}\frac{\omega}{2}$ ... (10)

In the graphical approach, θ_{L_1} describes a circular path, whereas θ_{L_2} follows a straight-line trajectory. Meanwhile θ_{L_3}also moves along a straight line, but in the direction opposite to that of θ_{L_2}. The circle has a radius of:

$$r = \frac{1}{2\sin\theta_{L_1}}$$

and the centre is at

$$\left(0.5, \frac{-1}{2\tan\theta_{L_1}}\right) \ldots (11)$$

The intersection of the circle and the straight line occurs at the point (u_i, v_i). This point can be determined using the following approach:

$$u_i = \frac{v_i}{\tan\theta_{L_2}} - 1 \quad \ldots (12)$$

& $v_i =$

$$\frac{3\cot\theta_{L_2} + \cot\theta_{L_1} \pm \sqrt{(3\cot\theta_{L_2} + \cot\theta_{L_1})^2 - 8csc^2\theta_{L_2}}}{2csc^2\theta_{L_2}} \ldots (13)$$

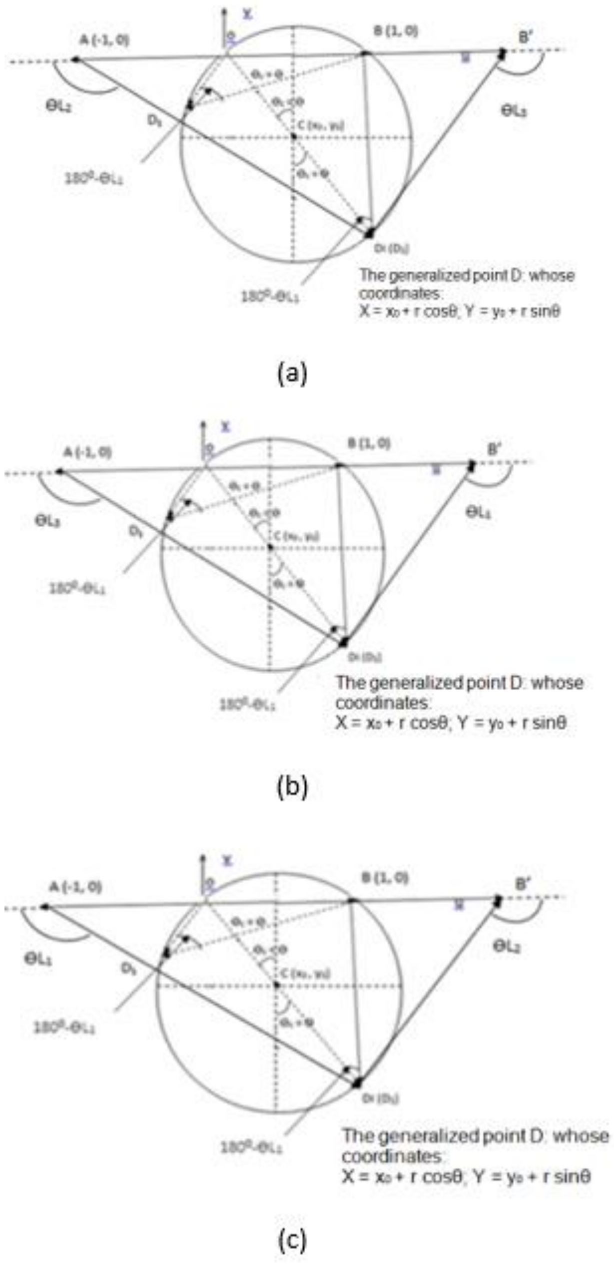

Fig. 3: Illustrates the normalised phase diagrams for three different parameter sets. (a) For Set 1, coefficients C1 and C2 are negative, while C3 is positive. (b) For Set 2, C2 and C3 take negative values, whereas C1 is positive. (c) For Set 3, C3 and C1 are negative, while C2 is positive.

Using ω as a constant, the NPD corresponding to the three subsystem sets are illustrated in Figure 3(a), (b), and (c). Each figure represents a distinct arrangement of the subsystems under consideration. The limit cycle conditions can be analyzed using any one of these sets. Similarly, the associated system parameters can be evaluated from each configuration.

$$N_2 = (11-3\omega^2)\omega^2 \pm \sqrt{(11-3\omega^2)\omega^4 - 8(\omega^2+16)(1-\omega^2)^2\omega^2} \quad (14)$$

$$N_1 = \frac{(\omega^2-1)}{8} N_2 + \frac{9\omega^2-\omega^4}{8} \quad \cdots (15)$$

$$\frac{Xm_1}{Xm_2} = \frac{X_1}{X_2} = \frac{(1+\omega^2)\sqrt{[\omega^2(\omega^2+16-2N_2)+N_2^2]}}{2N_1\sqrt{\omega^2+16}} \quad \cdots (16)$$

$$\frac{X_1}{X_2} = \frac{BD_i}{AD_i} = \sqrt{\frac{(1-u_i)^2+(u_i)^2}{(1+u_i)^2+(u_i)^2}} \quad \cdots (17)$$

$$\theta_{L_1} = \theta N_1(Xm_1, \omega) + \theta G_1$$

$$\theta_{L_2} = \theta N_2(Xm_2, \omega) + \theta G_2$$

$$\theta_{L_3} = \theta N_3(Xm_3, \omega) + \theta G_3$$

Table 1(a) presents the values of θ_{L_1}, θ_{L_2}, θ_{L_3}, along with the radius (r), the circle's centre, and the points of intersection between the two straight lines and the circle for Sets 1, 2, and 3 corresponding to Example 1.

Table 1(b) presents the values of angular frequency ω, radius r, and the coordinates of the centre of the circle for Set 1 corresponding to Example 1 (rectangular hysteresis). The ratio, X1/X2 is taken from Table 1(a), where it is also obtained from the plot as: X1/X2= (BD')/(AD') Similarly, the ratio Xm1/Xm3=X1/X3 is taken from Table 1(a), and from the plot it is expressed as X1/X3= BD'/B'D'. These relations are used for determining the required parameters listed in Table 1(b).

The values listed in Table 1 represent the ratios X_1/X_2 evaluated for different values of ω, obtained both analytically using Eqn. (16) and graphically from the normalised phase diagrams. Agreement between the analytical values of X_1/X_2 and those determined from the graphical ratio (BD′/AD′) verifies the existence of a limit cycle.

2.1.2 Example: 2

The system under consideration is illustrated in Figure 1. It consists of three linear dynamic elements represented by their transfer functions. The transfer functions are given by

$$G_1(s) = \frac{2}{s(s+1)^2}$$

$$G_2(s) = \frac{1}{s(s+4)}$$

$$G_2(s) = \frac{1}{s(s+2)}$$

In addition to these linear elements, the system also contains three nonlinear (NL) elements. Each of these nonlinear elements exhibits backlash characteristics. The backlash widths are identical for all three elements, with $b_1=b_2=b_3=1$. The characteristics of these nonlinear elements are shown in Figure 4(a), Figure 4(b), and Figure 4(c), respectively.

Table 1(a): Calculated Numerical Parameters for Set 1 of Example 1

ω	**N_1**	**N_2**	**N_3**	**X_{m1}**	**X_{m2}**	**X_{m3}**	**θ_{L1}**	**θ_{L2}**	**θ_{L3}**	**Radius r**	**Centre $(0.5, \frac{-1}{2\tan\theta_{L_1}})$**
0.60	0.35	0.45	0.45	3.15	3.61	3.61	-161.00	-106.40	-114.60	1.580	0.5, -1.46
0.61	0.36	0.46	0.46	3.07	3.49	3.49	-162.10	-106.90	-115.20	1.630	0.5, -1.55
0.62	0.37	0.47	0.47	2.99	3.37	3.37	-163.10	-107.30	-115.70	1.730	0.5, -1.66
0.63	**0.38**	**0.48**	**0.48**	**2.92**	**3.26**	**3.26**	**-164.10**	**-107.70**	**-116.20**	**1.830**	**0.5, -1.76**
0.64	0.40	0.50	0.50	2.85	3.16	3.16	-166.30	-108.10	-116.80	2.110	0.5, -2.05
0.65	0.41	0.51	0.51	2.78	3.06	3.06	-166.30	-108.60	-117.40	2.120	0.5, -2.06
0.70	0.48	0.57	0.57	2.47	2.62	2.62	-171.60	-110.80	-120.20	3.470	0.5, -3.40

Table 1(b). presents the graphically constructed phase diagrams for Example 1 (rectangular hysteresis), showing the variation of ω and the corresponding values of r for Set 1.

ω	**Radius r**	**Centre $\left(0.5, \frac{-1}{2\tan\theta_{L_1}}\right)$**	$\frac{X_1}{X_2} = \frac{BD'}{AD'}$ **From plot**	$\frac{X_1}{X_2} = \frac{Xm_1}{Xm_2}$ **From Table 1a**	$\frac{X_1}{X_3} = \frac{BD'}{B'D'}$ **from plot**	$\frac{Xm_1}{Xm_3}$ **From the Table 1a**	**Phasor Diagram**
0.60	1.58	0.5, -1.46		0.87		0.87	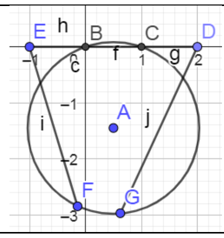
0.63	**1.83**	**0.5, -1.76**	**0.97**	**0.90**	**0.91**	**0.90 (The results were found to be consistent with the values obtained from the plot.)**	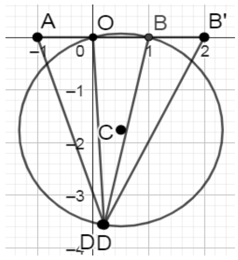 **OD' = 3.5 = C_1/R_1 = C_1** **OA = 1 = C_2** **BB' = 1= C_3** **BD' = 3.6 = X_1** **AD' = 3.7 = X_2** **B'D'=3.9 = X_3** **X_1/X_2 = BD'/AD' = 0.97** **X_1/X_3 = BD'/B'D' = 0.91**
0.64	2.11	0.5, -2.05		0.90		0.90	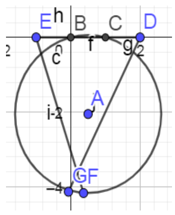
0.65	2.12	0.5, -2.06		0.91		0.91	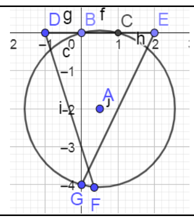

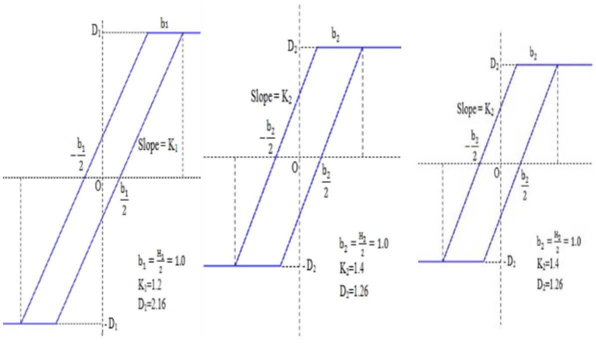

(a) (b) (c)

Fig. 4: Transfer characteristics illustrating how inputs are mapped to outputs for the NL elements, N_1, N_2 and N_3.

The describing functions corresponding to the above backlash-type nonlinear elements can be represented as follows:

$$N(X_m, \omega) = \left\{\frac{K}{\pi}\sqrt{(\frac{\pi}{2} + \beta + \frac{1}{2}sin2\,\beta)^2 + \cos^4\beta}\right\} \angle - \tan^{-1}\left(\frac{\cos^2\beta}{\frac{\pi}{2}+\beta+\frac{1}{2}sin2\,\beta}\right) \quad \text{for} \quad X_m > \frac{b}{2}$$

$$= 0 \quad for\, X_m < \frac{b}{2} \; .... (18)$$

$$N_1(X_{m1}, \omega) = \frac{K_1}{\pi}\sqrt{(\frac{\pi}{2} + \beta_1 + \frac{1}{2}sin2\,\beta_1)^2 + \cos^4\beta_1} \; .... (19)$$

$$N_2(X_{m2}, \omega) = \frac{K_2}{\pi}\sqrt{(\frac{\pi}{2} + \beta_2 + \frac{1}{2}sin2\,\beta_2)^2 + \cos^4\beta_2} \; .... (20)$$

$$N_3(X_{m3}, \omega) = \frac{K_3}{\pi}\sqrt{(\frac{\pi}{2} + \beta_3 + \frac{1}{2}sin2\,\beta_3)^2 + \cos^4\beta_3} \; .... (21)$$

The derivative of the describing function is obtained as follows:

$$N_1{}'(X_{m1}, \omega) = \frac{K_1}{\pi} \times \frac{1}{\sqrt{(\frac{\pi}{2}+\beta_1+{}^1\!/_2\sin 2\,\beta_1)^2+cos^4\beta_1}} \times (2 \times \left(\frac{\pi}{2} + \beta_1 + \frac{1}{2}\sin 2\,\beta_1\right) + (1 + \cos 2\beta_1) + 2 \times (\cos 2\beta_1 + 1) \times (-2sin^2\,\beta_1)) \quad ... \quad (22)$$

$$f_1(X_{m1}) = \frac{K_1}{\pi}\sqrt{(\frac{\pi}{2} + \beta_1 + {}^1\!/_2\sin 2\,\beta_1)^2 + cos^4\beta_1} - N_1(X_{m1}) \quad ... \quad (23)$$

$$f_1{}'(X_{m1}) = \frac{K_1}{\pi} \times \frac{1}{\sqrt{(\frac{\pi}{2}+\beta_1+{}^1\!/_2\sin 2\,\beta_1)^2+cos^4\beta_1}} \times (2 \times \left(\frac{\pi}{2} + \beta_1 + \frac{1}{2}\sin 2\,\beta_1\right) + (1 + \cos 2\beta_1) + 2 \times (\cos 2\beta_1 + 1) \times (-2sin^2\,\beta_1))\, N_1{}'(X_{m1}) \quad ... \; (24)$$

Again,

$$N_2(X_{m2}, \omega) = \frac{K_2}{\pi}\sqrt{(\frac{\pi}{2} + \beta_2 + {}^1\!/_2\sin 2\,\beta_2)^2 + cos^4\beta_2} \quad ... \quad (25)$$

$$N_2{}'(X_{m2}, \omega) = \frac{K_2}{\pi} \times \frac{1}{\sqrt{(\frac{\pi}{2}+\beta_2+{}^1\!/_2\sin 2\,\beta_2)^2+cos^4\beta_2}} \times (2 \times \left(\frac{\pi}{2} + \beta_2 + \frac{1}{2}\sin 2\,\beta_2\right) + (1 + \cos 2\beta_2) + 2 \times (\cos 2\beta_2 + 1) \times (-2sin^2\,\beta_2)) \quad ... \quad (26)$$

$$f_2(X_{m2}) = \frac{K_2}{\pi}\sqrt{(\frac{\pi}{2} + \beta_2 + {}^1\!/_2\sin 2\,\beta_2)^2 + cos^4\beta_2} - N_2(X_{m2}) \quad ... \quad (27)$$

$$f_2{}'(X_{m2}) = \frac{K_1}{\pi} \times \frac{1}{\sqrt{(\frac{\pi}{2}+\beta_2+{}^1\!/_2\sin 2\,\beta_2)^2+cos^4\beta_2}} \times \left(2\left(\frac{\pi}{2} + \beta_2 + \frac{1}{2}\sin 2\,\beta_2\right) + (1 + \cos 2\beta_2) + 2(\cos 2\beta_2 + 1) \times (-2sin^2\,\beta_2)\right) - N_1{}'(X_{m1}) \quad ... \quad (28)$$

The relationships between N_1–X_1, N_2–X_2, and N_3–X_3 are implicit, transcendental in nature, and exhibit memory-type behaviour. Therefore, the third solution procedure described in [46] is adopted. In Eqs. (23), (25), and (27), the NL elements N_1, N_2, and N_3 appear in absolute form. For a fixed value of ω, these NL terms remain constant.

The ratios X_2/X_1 and X_3/X_1 are computed using the NR method and subsequently compared with the corresponding ratios obtained from the graphical representation of the normalised phase diagrams. At ω=0.57 (see Table 2a), a close agreement between the analytical and graphical values is observed, confirming the presence of a limit cycle.

While solving Eqs. (19)–(21) via the NR method, phase angles are not explicitly included during the iterative computation. However, they are incorporated into the overall loop phase, as reflected in Eqs. (29)–(31). At each iteration, the phase condition must be satisfied, given by $\theta = 180^o = \angle N_1 + \angle N_2 + \angle N_3 + \angle G_1 + \angle G_2 + \angle G_3$.

The normalised phase diagrams are developed for three separate parameter configurations:

- **Set 1:** Subsystems S_1, S_2, S_3 satisfy the conditions $C_1<0$, $C_2<0$, and $C_3>0$ as illustrated in Figure 5(a).
- **Set 2:** Subsystems S_1, S_2, S_3 correspond to $C_2<0$, $C_3<0$, and $C_1>0$ as shown in Figure 5(b).

- **Set 3:** Subsystems S_1, S_2, S_3 are defined by $C_3<0$, $C_1<0$, and $C_2>0$ as presented in Figure 5(c).

Table 2 presents the values of $\theta_{L_1}, \theta_{L_2}, \theta_{L_3}$, and the radius r, for Sets 1, 2, and 3 corresponding to Example 2. It also includes the coordinates of the intersection points formed between the two straight lines and the circle for each parameter set. These values are used for the analysis and comparison of the system behaviour under the three different configurations.

$$\theta_{L_1} = \theta_{N_1(X_{m1},\omega)} + \theta_{G_1}$$
$$\theta_{L_2} = \theta_{N_2(X_{m2},\omega)} + \theta_{G_2}$$
$$\theta_{L_3} = \theta_{N_3(X_{m3},\omega)} + \theta_{G_3}$$
$$r_1 = \frac{1}{2\sin\theta_{L_1}}$$

and centre is given by:

$$C\left(\frac{1}{2}\right) - \frac{1}{2\tan\theta_{L_1}}$$

For set 1:

$$\theta_{L_1} = [-tan^{-1}\left(\frac{cos^2\beta_1}{\frac{\pi}{2}+\beta_1+\frac{1}{2}sin^2\beta_1}\right) - \frac{\pi}{2} - 2tan^{-1}\omega] \quad ,$$

$$\beta_1 = sin^{-1}(1-\frac{b_1}{X_{m1}}); \qquad (29)$$

$$\theta_{L_2} = [-tan^{-1}\left(\frac{cos^2\beta_2}{\frac{\pi}{2}+\beta_2+\frac{1}{2}sin^2\beta_2}\right) - \frac{\pi}{2} - tan^{-1}\frac{\omega}{4}],$$

$$\beta_2 = sin^{-1}(1-\frac{b_2}{X_{m2}}) \qquad (30)$$

$$\theta_{L_3} = [-tan^{-1}\left(\frac{cos^2\beta_3}{\frac{\pi}{2}+\beta_3+\frac{1}{2}sin^2\beta_3}\right) - \frac{\pi}{2} - tan^{-1}\frac{\omega}{2}],$$

$$\beta_3 = sin^{-1}(1-\frac{b_3}{X_{m3}}) \qquad (31)$$

$$\frac{C_1}{R_1} = \frac{C_1}{C_2} = \frac{Y_1G_1}{Y_2G_2} = \frac{X_{m1}N_1G_1}{X_{m2}N_2G_2} \qquad (32)$$

Or $$\frac{C_1}{R_1} = \frac{(X_{m1}G_1)\frac{K_1}{\pi}\sqrt{(\frac{\pi}{2}+\beta_1+{}^1/_2\sin 2\beta_1)^2+cos^4\beta_1}}{(X_{m2}G_2)\frac{K_2}{\pi}\sqrt{(\frac{\pi}{2}+\beta_2+{}^1/_2\sin 2\beta_2)^2+cos^4\beta_2}} \qquad (33)$$

Or$$\frac{C_1}{R_1} = \frac{(K_1X_{m1}G_1)\sqrt{(\frac{\pi}{2}+\beta_1+{}^1/_2\sin 2\beta_1)^2+cos^4\beta_1}}{(K_2X_{m2}G_2)\sqrt{(\frac{\pi}{2}+\beta_2+{}^1/_2\sin 2\beta_2)^2+cos^4\beta_2}} \qquad (34)$$

Y_1, Y_2, N_1, and N_2 denote the amplitudes of the corresponding sinusoidal signals, while G_1 & G_2 represent the magnitudes (absolute values) of their respective transfer functions.

From Fig. 4, $K_1 = 1.2$, and $K_2 = K_3 = 1.4$

Since, $|G_1(j\omega)| = \frac{2}{\omega(\omega^2+1)}$; $|G_2(j\omega)| = \frac{1}{\omega\sqrt{16+\omega^2}}$;

$$\left|\frac{G_1}{G_2}\right| = \frac{2\sqrt{16+\omega^2}}{(\omega^2+1)}$$

Eq. (34) can be written as:

$$\frac{C_1}{R_1} = \frac{1.714\times X_{m1}\sqrt{16+\omega^2}}{X_{m2}(\omega^2+1)}\frac{\sqrt{(\frac{\pi}{2}+\beta_1+{}^1/_2\sin 2\beta_1)^2+cos^4\beta_1}}{\sqrt{(\frac{\pi}{2}+\beta_2+{}^1/_2\sin 2\beta_2)^2+cos^4\beta_2}}$$

(35)

$$\frac{C_1}{C_3} = \frac{(K_1X_{m1}G_1)\sqrt{(\frac{\pi}{2}+\beta_1+{}^1/_2\sin 2\beta_1)^2+cos^4\beta_1}}{(K_3X_{m3}G_3)\sqrt{(\frac{\pi}{2}+\beta_3+{}^1/_2\sin 2\beta_3)^2+cos^4\beta_3}}$$

$$= \frac{1.714\times X_{m1}\sqrt{4+\omega^2}}{X_{m2}(\omega^2+1)}\frac{\sqrt{(\frac{\pi}{2}+\beta_1+{}^1/_2\sin 2\beta_1)^2+cos^4\beta_1}}{\sqrt{(\frac{\pi}{2}+\beta_3+{}^1/_2\sin 2\beta_3)^2+cos^4\beta_3}} \qquad (36)$$

In accordance with [46] the normalized phase diagrams, for 3×3 systems, are constructed using three distinct sets to illustrate the limit cycle conditions, as depicted in Figure 5(a), (b), and (c).

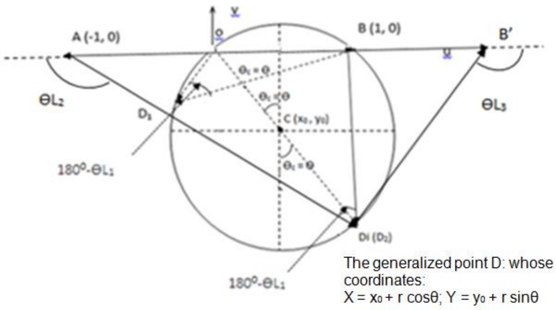

Fig. 5(a): Geometrical representation of the normalized phase diagram with $C_1<0$, $C_2<0$, and $C_3>0$ (set 1)

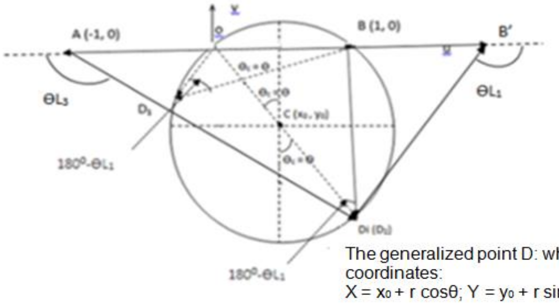

Fig. 5(b): Geometrical representation of the normalized phase diagram with $C_2<0$, $C_3<0$, and $C_1>0$ (set 2)

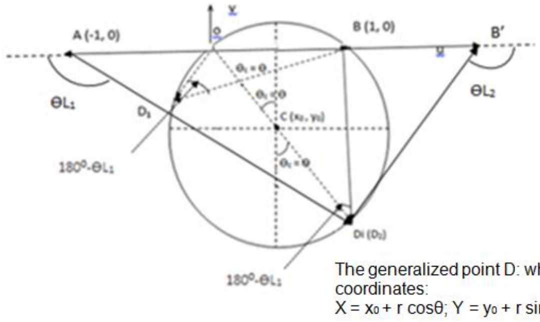

Fig. 5(c): Geometrical representation of the normalized phase diagram with $C_3<0$, $C_1<0$, and $C_2>0$ (set 3)

Table 2(a) presents the values ω, N_1, N_2, N_3, X_{m1}, X_{m2}, X_{m3}, for Set 1 corresponding to Example 4 (Backlash). It also includes the values of θ_{L_1}, θ_{L_2}, θ_{L_3}, the radius r, and the coordinates of the circle's centre.

From graphical plot, we obtain

$$\frac{X_2}{X_1} = \frac{AD'}{BD'}$$

And from NR method, we get

$$\frac{X_{m2}}{X_{m1}} = \frac{X_2}{X_1}$$

Also from graphical and NR method respectively, we get the following equations:

$$\frac{X_3}{X_1} = \frac{B'D'}{BD'}$$

$$\frac{X_{m3}}{X_{m1}} = \frac{X_3}{X_1}$$

It may be noted that Table 2 presents the values of Eqn. (38) for different values of ω. These values are obtained using Eqn. (38) as well as from the graphical representation of the Normalised Phase Diagrams. When the ratio $\frac{X_2}{X_1}$ computed from Eqn. (38) agrees with the corresponding value $\frac{AD'}{BD'}$ obtained from graphical plot, the limit cycle condition is satisfied. Similarly, the condition, Eqn. (40) is evaluated using Eq. (39), is verified when it matches the graphical ratio $\frac{B'D'}{BD'}$ thereby confirming the existence of limit cycles.

Table 2(b) presents the values of the radius r, and the coordinates of the circle's centre for Set 1 corresponding to Example 2 (Backlash).

2.2 Simulation using MATLAB

I. Program with MATLAB Code

Examples 1 and 2 are reconsidered within a 3×3 system (shown in Figure 1), which consists of three NL elements (as detailed in Figures 2 and 4, respectively) together with three linear transfer functions.

By Partial Fraction Expansion of $G_1(s)$, $G_2(s)$ and $G_3(s)$:

$$G_1(s) = \frac{2}{s} - \frac{2}{s+1} - \frac{2}{(s+1)^2}$$

$$: \frac{2}{s}, \frac{-2}{s+1}, \frac{-2}{s+1}\left(\frac{1}{s+1}\right)$$

$$G_2(s) = \frac{0.25}{s} - \frac{0.25}{s+4}$$

$$G_3(s) = \frac{0.5}{s} - \frac{0.5}{s+2}$$

For a small sampling period, T, TG(z) ≈ G(s). Figures 6 and 7 present the canonical and discrete (digital) representations for Examples 1 and 2.

Figure 8 shows the Simulink-based simulation model for investigating limit cycles in Example 1 involving rectangular hysteresis

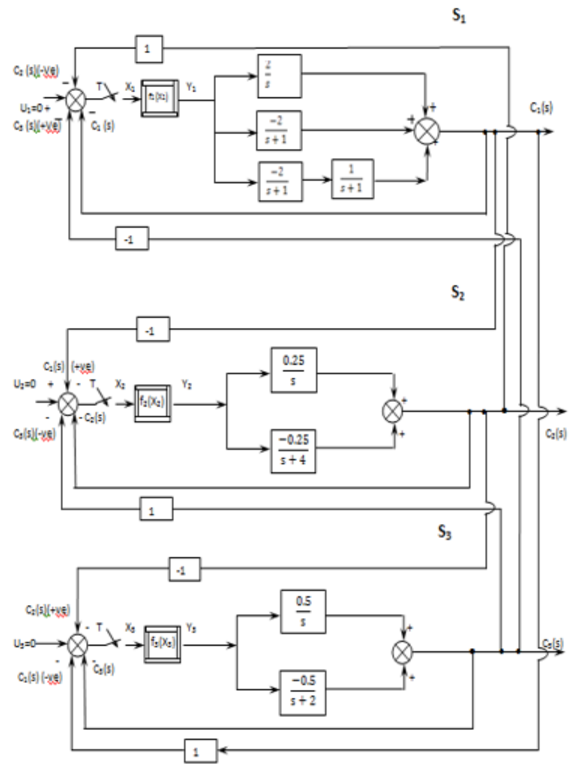

Fig. 6: Block diagram of a multi-loop control system consisting of three interconnected subsystems (S_1 , S_2 , and S_3), each implementing feedback control with dynamic compensators and transfer function elements, sharing common input signals and producing the output C(s)

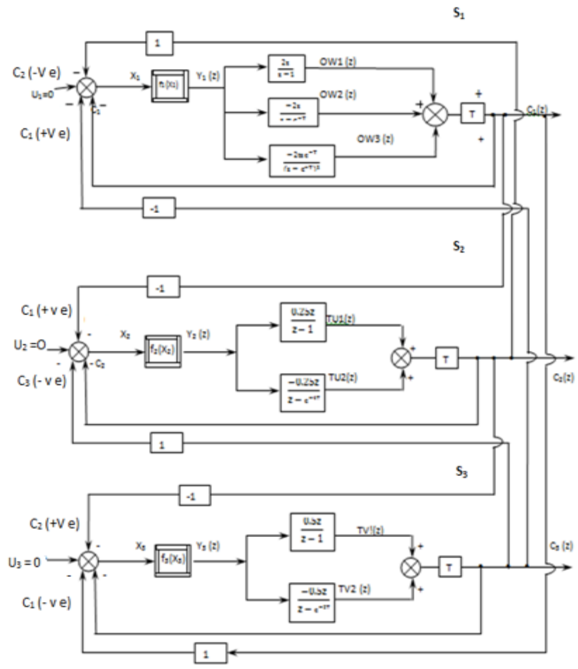

Fig. 7: The Digital representation of a hierarchical multi-loop control system composed of three subsystems (S_1 , S_2 , and S_3), showing feedback interconnections, controller transfer functions, and signal flow paths leading to the combined output C(s).

Table 2(a). Numerical Results of Various Parameters for Example 2

ω	X_{m1}	X_{m2}	X_{m3}	N_1	N_2	N_3	θ_{L1}	θ_{L2}	θ_{L3}	Radius r	$\frac{X_{m3}}{X_{m1}}$	$\frac{X_{m2}}{X_{m1}}$
0.52	3.85	2.85	2.85	1.30	1.26	1.26	-154.4	-110.8	-117.8	-1.18	0.74	0.74
0.55	3.57	2.55	2.55	1.11	1.25	1.25	-157.9	-112.5	-120.0	-1.32	0.72	0.72
0.570	**3.30**	**2.30**	**2.30**	**1.29**	**1.23**	**1.23**	**-160.6**	**-114.3**	**-122.18**	**-1.51**	**0.93**	**0.93**
0.575	3.27	2.25	2.25	1.28	1.22	1.22	-161.1	-114.8	-122.6	-1.55	0.69	0.69
0.60	2.97	1.95	1.95	0.25	1.71	1.71	-164.4	-117.6	-128.3	-1.86	0.65	0.65
0.62	2.63	1.67	1.67	0.28	1.79	1.79	-168.1	-120.1	-129.3	-2.44	0.63	0.63
0.65	2.34	1.47	1.47	0.31	1.86	1.86	-172.0	-123.9	-132.7	-3.61	0.62	0.62
0.67	2.34	1.43	1.43	0.311	2.57	2.57	-174.0	-124.9	-133.9	-4.81	0.61	0.61
0.695	2.34	1.47	1.4	0.30	3.24	3.24	-175.6	-125.1	-134.5	-6.56	0.62	0.62
0.696	2.34	1.43	1.4	0.305	3.26	3.26	-175.6	-125.2	-134.5	-6.62	0.61	0.61
0.70	2.34	1.43	1.43	0.30	3.38	3.384	-175.9	-125.2	-134.6	-7.12	0.62	0.62

Table 2(b): Normalized phase diagrams obtained graphically for various values of angular frequency ω together with the corresponding amplitude ratios and radius r for Example 2 with backlash nonlinearity.

ω	Radius r	Centre $(0.5, \frac{-1}{2\tan\theta_{L_1}})$	$\frac{X_{m2}}{X_{m1}}$ *from plot*	$\frac{X_{m2}}{X_{m1}}$ *from* Table 2a	$\frac{X_{m3}}{X_{m1}}$ from plot	$\frac{X_{m3}}{X_{m1}}$ From Table 2a	Phasor Diagram
0.52	-1.1	0.5, -1.0		0.7		0.7	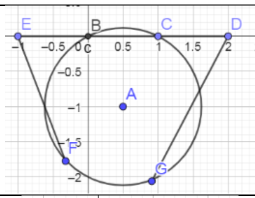
0.55	-1.3	0.5, -1.2		0.71		0.71	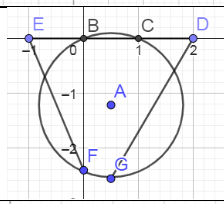
0.57	**-1.5**	**0.5, -1.4**	**1.07**	**1.0**	**1.13**	**1.13**	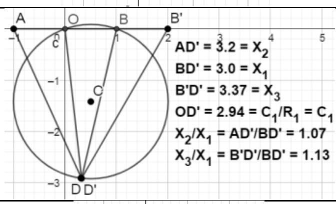
0.60	-1.8	0.5, -1.7		0.65		0.65	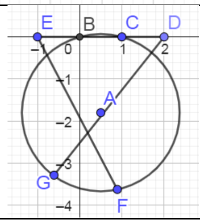

0.62	2.4	0.5, -2.3		0.63		0.63	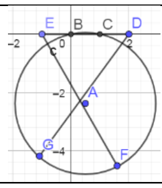

Z-transfer functions from Laplace functions:

$$G_1(s): \frac{2.0}{s} \Rightarrow \frac{2z}{z-1};$$
$$\frac{-2.0}{s+1} \Rightarrow \frac{-2z}{z-e^{-T}};$$
$$\frac{-2.0}{(s+1)^2} \Rightarrow \frac{-2Tz\,e^{-T}}{(z-e^{-T})^2}$$
$$G_2(s): \frac{0.250}{s} \Rightarrow \frac{0.25z}{(z-1)};$$
$$\frac{-0.250}{s+4} \Rightarrow \frac{-0.25z}{z-e^{-4T}};$$
$$G_3(s): 0.5s \Rightarrow 0.5z(z-1);$$
$$-0.5s + 2.0 \Rightarrow -0.5z - e^{-2T}$$

In Z-domain, we have,

$$\frac{\mathrm{W1(z)}}{\mathrm{Y_1(z)}} = \frac{2\mathrm{z}}{\mathrm{z}-1}$$

W1 (nT) $=$ 2Y1 (nT) $+$ W1$(\overline{\mathrm{n}-1}\mathrm{T})$ .. (41)

$$\frac{\mathrm{W2(z)}}{\mathrm{Y_1(z)}} = \frac{-2\mathrm{z}}{\mathrm{z}-\mathrm{e}^{-\mathrm{T}}}$$

W2 (nT) = -2Y_1 (nT) +e^{-T} W2$(\overline{\mathrm{n}-1}\mathrm{T})$ .. (42)

$$\frac{\mathrm{W3(z)}}{\mathrm{Y_1(z)}} = \frac{-2\mathrm{Tze}^{-\mathrm{T}}}{(\mathrm{z}-\mathrm{e}^{-\mathrm{T}})^2}$$

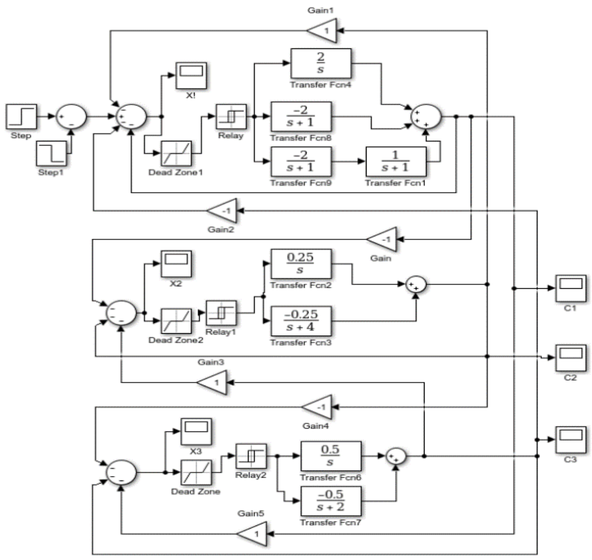

Fig. 8: A Simulink-based simulation model for investigating limit cycles in Example 1 involving rectangular hysteresis.

W3 (nT)

$= -2\mathrm{T}e^{-\mathrm{T}}\mathrm{Y}_1(\overline{\mathrm{n}-1}\mathrm{T}) + 2e^{-\mathrm{T}}\,\mathrm{W3}(\overline{\mathrm{n}-1}\mathrm{T}) - e^{-2\mathrm{T}}\mathrm{W3}\,(\overline{\mathrm{n}-2}\mathrm{T})$ … (43)

$$\frac{TU1(z)}{Y_2(z)} = \frac{0.25z}{(z-1)}$$

U1 (nT) $=$ 0.25Y2 (nT) $+$ U1$(\overline{\mathrm{n}-1}\mathrm{T})$.. (44)

$\frac{TU2(z)}{Y_2(z)} = \frac{-0.25z}{(z-e^{-4T})}$ whence U2 (nT) = -0.25Y_2 (nT) + e^{-4T}U2$(\overline{\mathrm{n}-1}\mathrm{T})$ -- (45)

$\frac{TV1(z)}{Y_3(z)} = \frac{0.5z}{(z-1)}$ whence V1 (nT) =0.5Y_3 (nT) +V1$(\overline{\mathrm{n}-1}\mathrm{T})$ -- (46)

$\frac{V2(z)}{Y_3(z)} = \frac{-0.5z}{(z-e^{-2T})}$ whence V2 (nT) = AK2* V2$(\overline{\mathrm{n}-1}\mathrm{T})-0.5Y_3$ (nT) -- (47)

Let $(\overline{\mathrm{n}-1}\mathrm{T})$ be taken as the zeroth instant. Then nT may be considered as the first instant, and therefore we have:

W1$(\overline{\mathrm{n}-1}\mathrm{T})$ = W1N0⇒W1N; W1 (nT) = W1N1; W2$(\overline{\mathrm{n}-1}\mathrm{T})$ = W2N0⇒W2N; W2 (n T) = W2N1

W3$(\overline{\mathrm{n}-2}\mathrm{T})$ = W3N (-1)⇒W3NN; W3 $(\overline{\mathrm{n}-1}\mathrm{T})$ = W3N0⇒ W3N ;

Now C_1(nT) = WN1 = T∗ [W1 (nT) +W2 (nT) + W3 (nT)]

Similarly, U1$(\overline{\mathrm{n}-1}\mathrm{T})$ = U1N0 ⇒ U1N;

Now C_2 (nT) =UN1= T* [0.25 Y_2 (nT) + U1N – 0.25Y_2 (nT) + AK3∗U2N]

Similarly, V1$(\overline{\mathrm{n}-1}\mathrm{T})$ = TV1N1

V2$(\overline{\mathrm{n}-1}\mathrm{T})$ = V2N1

Now C_3 (nT) = VN1 = C_3

Iterative process continues accordingly (Figure 9).

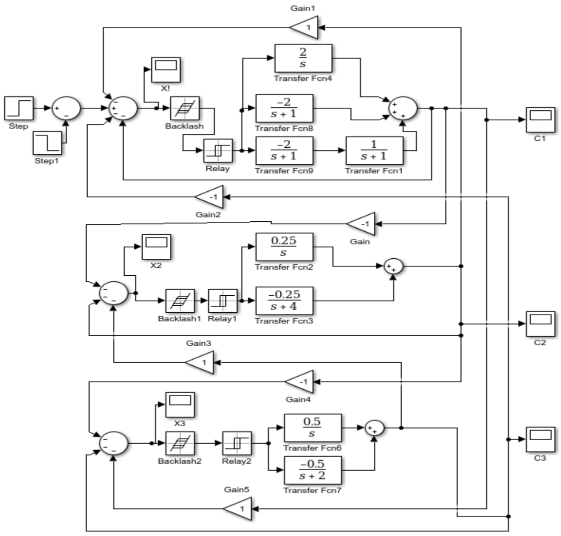

Fig. 9: A Simulink-based simulation model for investigating limit cycles in Example 2 involving backlash

2.3.1 Usage of SIMULINK

The values of X_1, X_2, X_3, C_1, C_2 & C_3 were computed using SIMULINK for both Examples 1 and 2. These plots were then validated by comparison with those obtained from digital simulation and the graphical method to assess the accuracy of the proposed approach.

Fig. 10(a) and Fig. 10(b) present the digital simulation and SIMULINK responses for Example 1, respectively. Fig. 11(a) and Fig. 11(b) show the corresponding responses for Example 2. All simulations were performed using a MATLAB code developed to implement the proposed procedure. The numerical results for Example 1 are summarized in Table 3(a). Similarly, the plots for Example 2 are presented in Table 3(b).

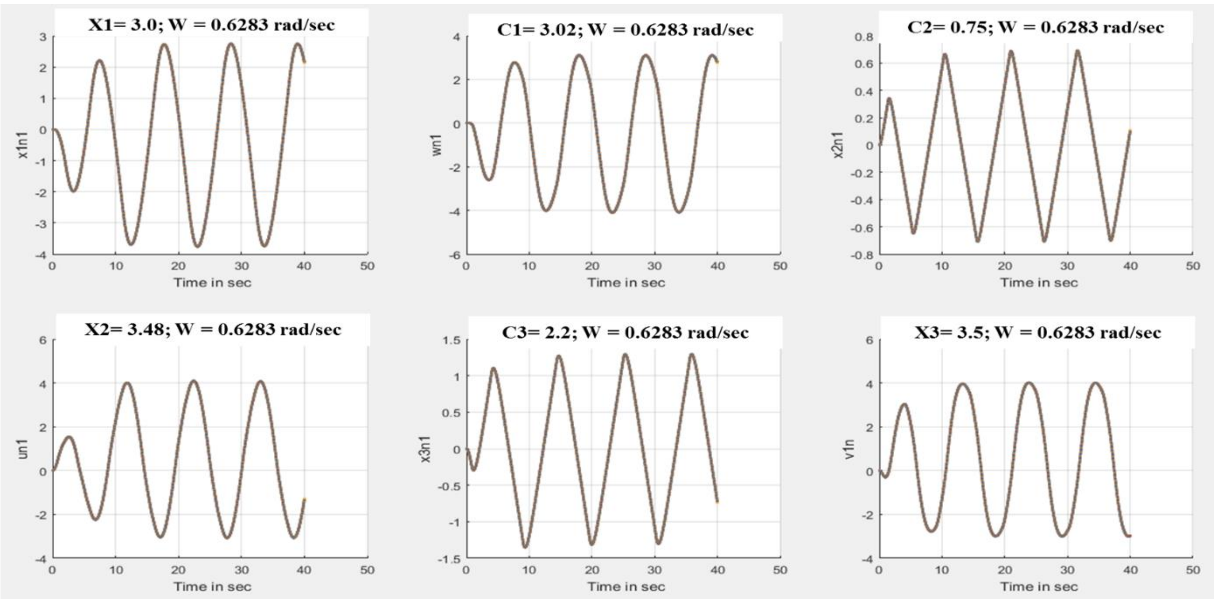

Fig. 10(a): The results of the digital simulation for Example 1, based on the rectangular hysteresis model, are presented along with their corresponding graphical outputs. The analysis focuses on the variables C_1, C_2, C_3, X_1, X_2 and X_3.

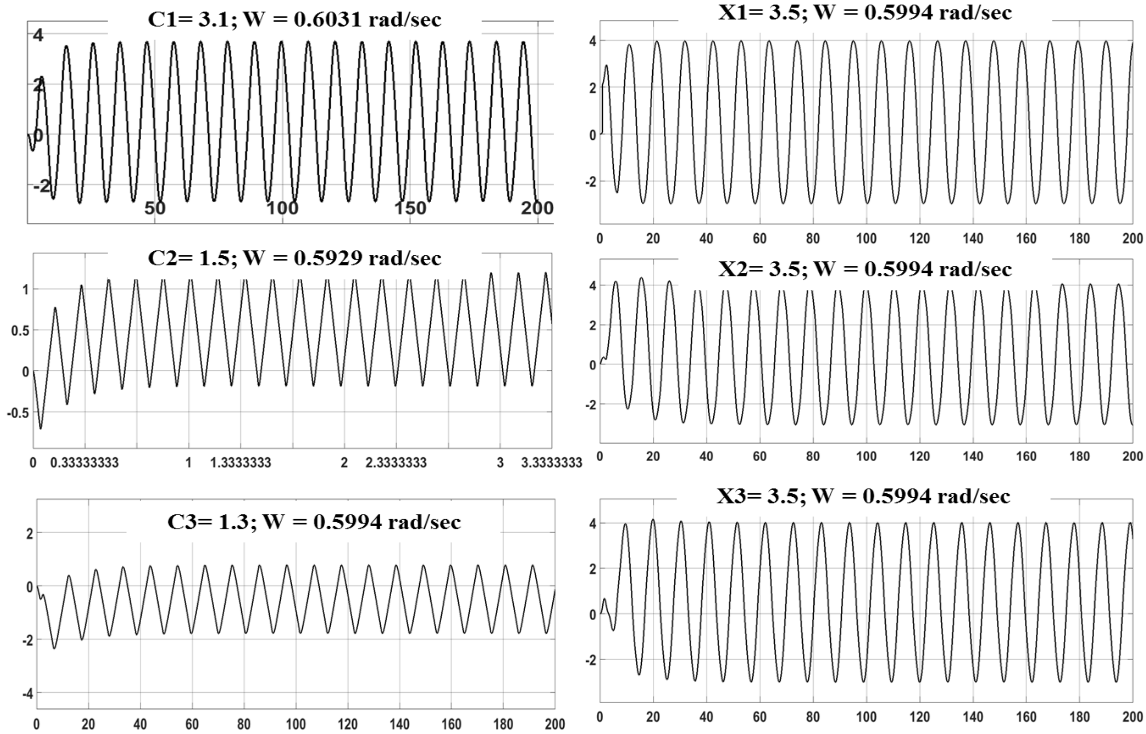

Fig. 10(b): Simulink results of Example 1, focusing on the rectangular hysteresis model. The analysis focuses on the variables C_1, C_2, C_3, X_1, X_2 and X_3.

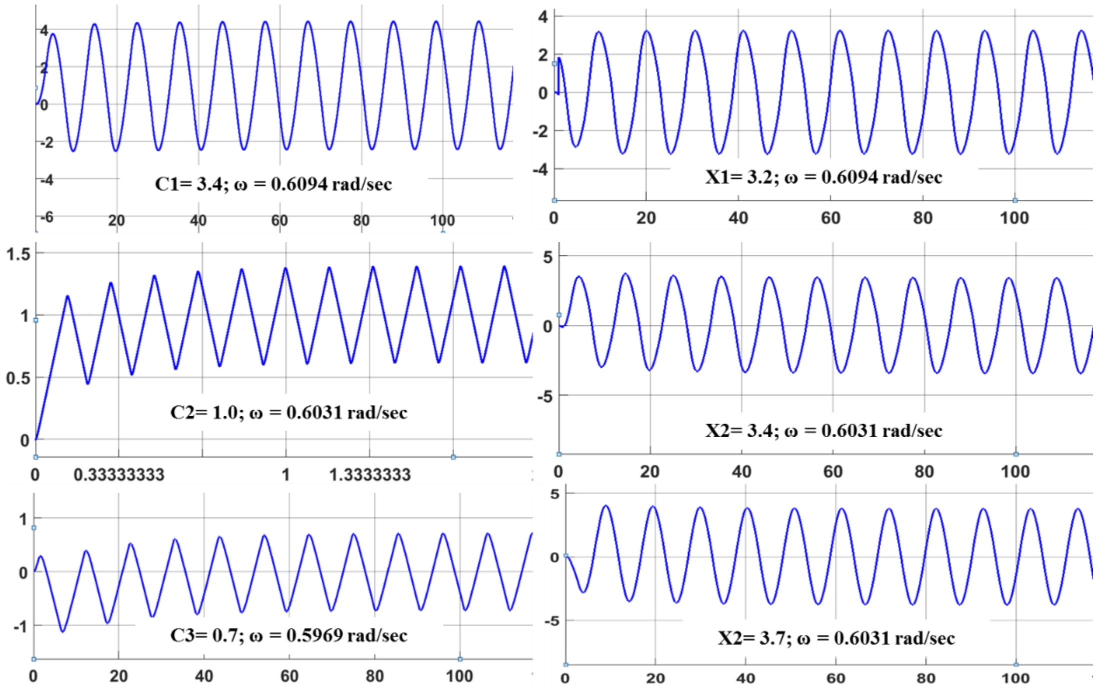

Fig. 11(a): The results of the digital simulation for Example 2, based on the backlash model are presented along with their corresponding graphical outputs. The analysis focuses on the variables C_1, C_2, C_3, X_1, X_2 and X_3.

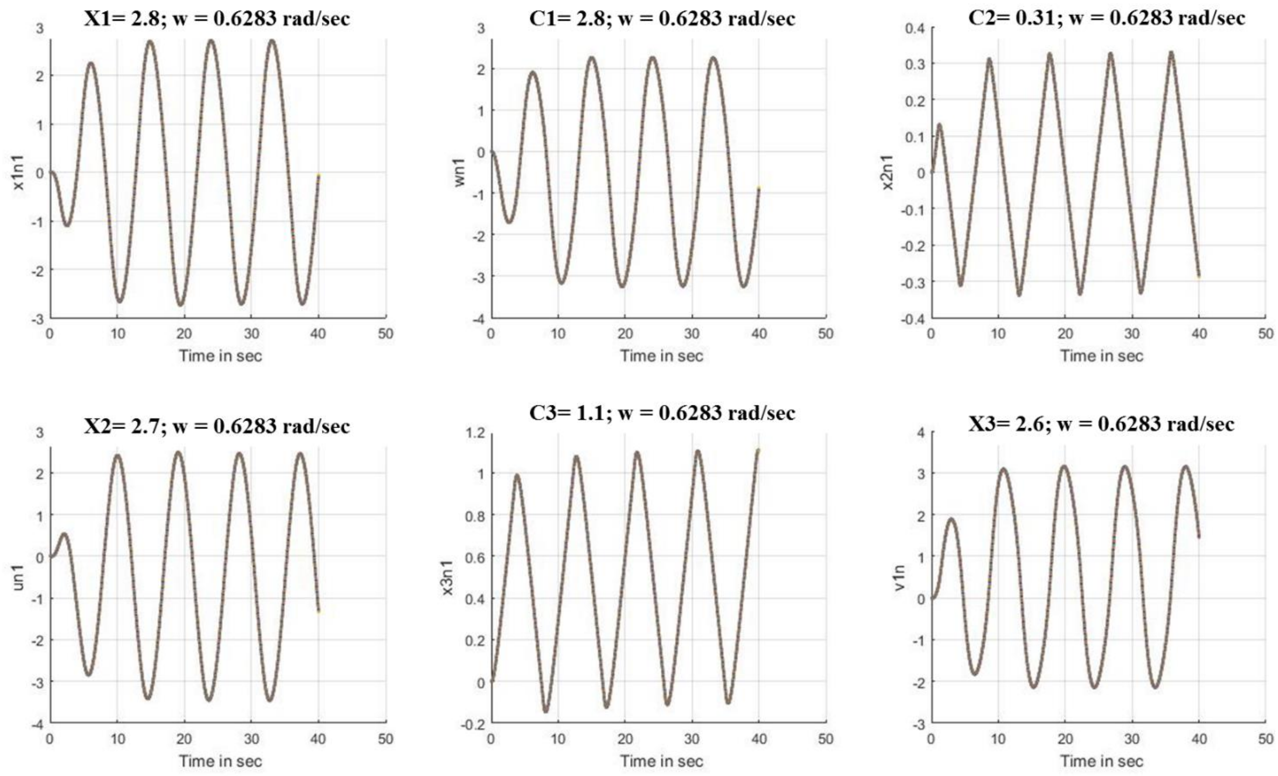

Fig. 11(b): The results of the simulink of Example 2, based on the backlash model are presented along with their corresponding graphical outputs. The analysis focuses on the variables C_1, C_2, C_3, X_1, X_2 and $X_{3/}$

Table 3(a). Comparative results for Example 1 (Rectangular Hysteresis) obtained through various analytical and simulation methods.

Sl. No	Technique	ω	X_1	X_2	X_3	C_1	C_2	C_3
1	Graphical	0.60	3.60	3.70	3.90	3.50	1.00	1.00
2	Simulation	0.60	3.00	3.40	3.50	3.00	0.70	1.30
3	SIMULINK	0.60	3.50	3.50	3.50	3.10	1.50	1.30

Table.3(b). Comparative results for Example 2 (Backlash) obtained through various analytical and simulation methods.

Sl. No	Technique	ω	X_1	X_2	X_3	C_1	C_2	C_3
1	Graphical	0.50	3.00	3.20	3.30	2.90	1.00	1.00
2	Simulation	0.60	2.80	2.70	2.60	2.80	0.30	1.10
3	SIMULINK	0.60	3.20	3.40	3.70	3.40	1.00	0.70

3. Signal Stabilization Analysis in a 3×3 NL system

3.1 Implementation of a Deterministic Signal Generation and Analysis

After confirming the existence of LC in the autonomous system, the quenching phenomenon was investigated by introducing high-frequency (HF) excitation signals ($\omega_f > 10\omega_s$) [5]. When the amplitude B1 of the forcing term B1 sin $\omega_f t$ was increased while keeping the remaining inputs constant or zero, the system exhibited complex oscillatory behaviour. These oscillations consisted of components at the forcing frequency ω_f, the natural limit-cycle frequency ω_s, and their combinations.

Consequently, the system response contained frequency components of the form $k_1\omega_f \pm k_2\omega_s$ where k_1, k_2 are integers [38, 46].
In the second configuration, identical forcing signals of the form B$\sin\omega_f t$ were applied simultaneously at all three input locations, namely U_1, U_2, & U_3, These sinusoidal inputs were introduced at the same time and with equal amplitude. The arrangement of this excitation scheme is illustrated in Figure 12(a) for Example 1. The corresponding configuration for Example 2 is shown in Figure 12(b). As the amplitude B was slowly increased, the limit-cycle frequency ω_s progressively shifted. Eventually, the system matched with the forcing frequency ω_f indicating suppression (quenching) of the limit cycle. Beyond this point, the system response was dominated by forced oscillations at ω_f.

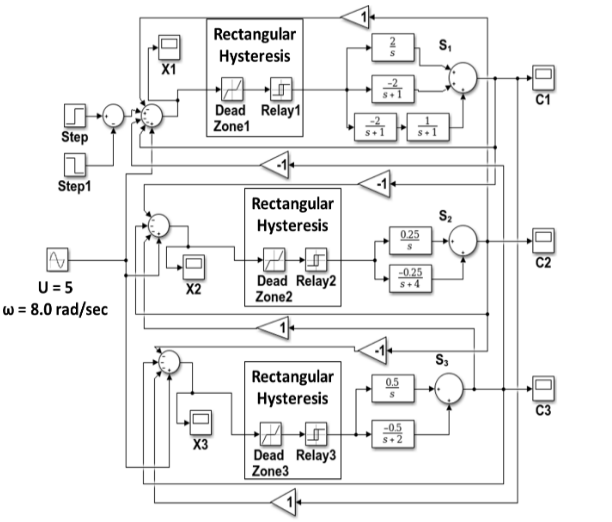

Fig. 12(a): SIMULINK model of the proposed multi-subsystem control structure showing three interconnected subsystems (S_1, S_2, and S_3) with rectangular hysteresis, dead-zone nonlinearities, and feedback loops used to generate outputs C_1, C_2, and C_3 under step input excitation.

The simulation results for signal stabilization under deterministic inputs for Example 1 and Example 2 are shown in Fig. 13 and Fig. 14, respectively.

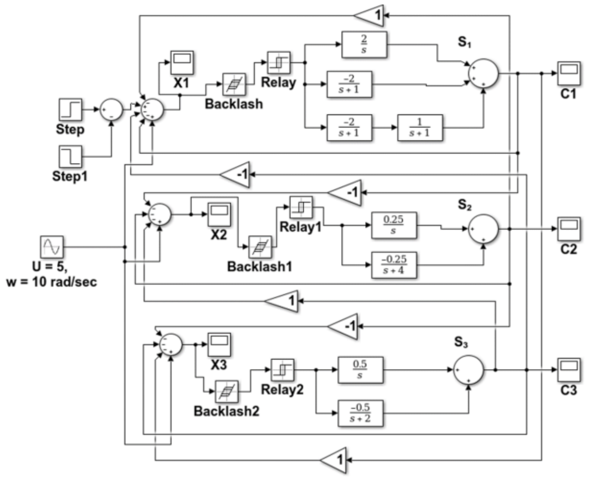

Fig. 12(b): Simulink block diagram of a multi-loop control system with step inputs, relay elements, backlash nonlinearities, and three subsystem outputs (C1, C2, C3), each governed by distinct transfer functions and feedback paths.

Figure 13 shows the steady-state values of the system variables as C_{1ss}, C_{2ss}, C_{3ss} and X_{1ss}, X_{2ss}, X_{3ss}.

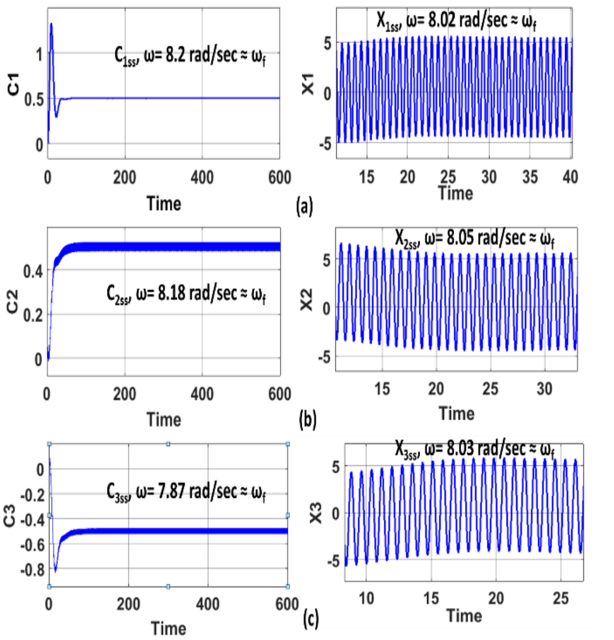

Fig. 13: Response of the system in Example 1 (rectangular hysteresis) when subjected to a deterministic input U = 5 sin(8t) with particular emphasis on the resulting forced oscillations and the associated stabilization of the system response.

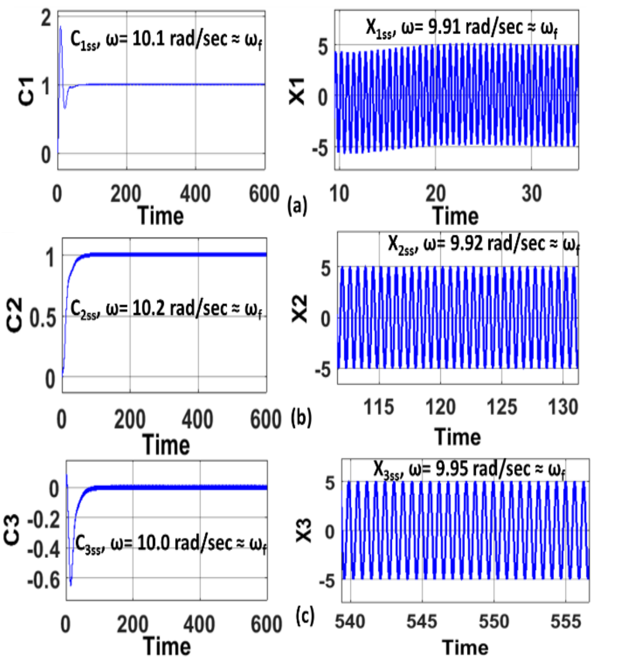

Fig. 14: The response of the system in Example 2 (Backlash) when subjected to a deterministic input U = 5 sin(10t) with particular emphasis on the resulting forced oscillations and the associated stabilization of the system response.

3.2 Implementation of a Gaussian signal

The concept of signal stabilization using Gaussian excitations has previously been examined for SISO NL systems [45, 47, 48]. More recent studies have emphasized robust analysis and design frameworks that explicitly account for uncertainty and stochastic effects. Despite these advances, the extension of Gaussian-based stabilization techniques to NL multivariable systems with memory—particularly even for 2×2 configurations—remained unresolved until it was addressed in [39].

In this work, that limitation is further explored by analyzing the suppression of LC in a 3×3 NL system subjected to stochastic excitation. Examples 1 and 2, which exhibit self-sustained oscillations under autonomous conditions, are revisited. To achieve stabilization and reduce these oscillations, Gaussian random inputs characterized by mean m and variance ϕ are applied at each input node. The results indicate that, for appropriate choices of m and ϕ, the limit cycle oscillations are effectively suppressed or significantly reduced. The corresponding simulation setups are depicted in Fig. 15(a) and Fig. 16(a) for Example 1 and Example 2, respectively, while the resulting system responses are presented in Fig. 15(b) and Fig. 16(b).

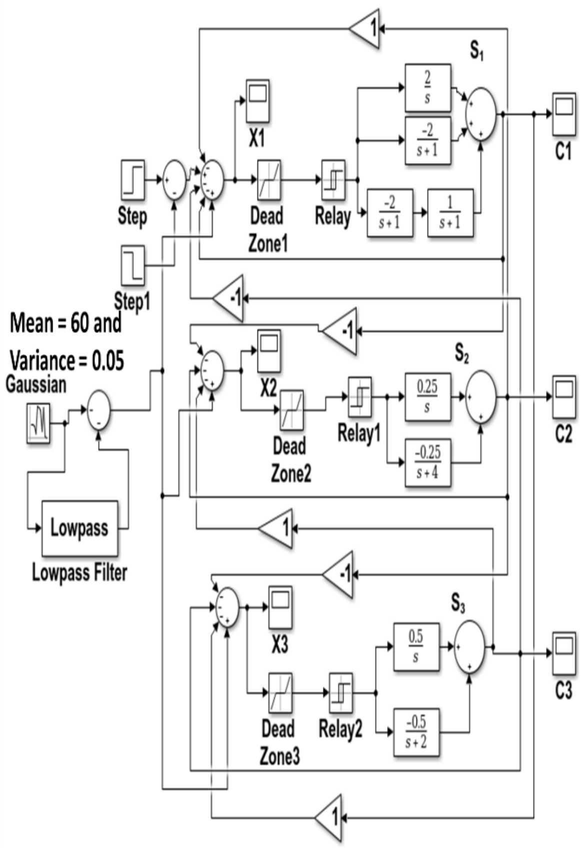

Fig. 15(a): System representation derived from Figure 9 used to study forced oscillatory behaviour in Example 3 (rectangular hysteresis) under a Gaussian excitation with mean 60.0 and variance 0.050.

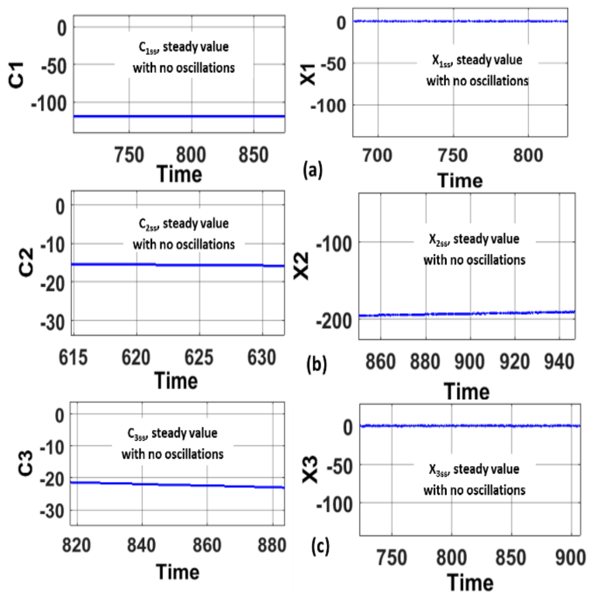

Fig. 15(b): Analysis of forced oscillations during signal stabilization under Gaussian excitation (mean 60.0, variance 0.050) for Example 3 with rectangular hysteresis.

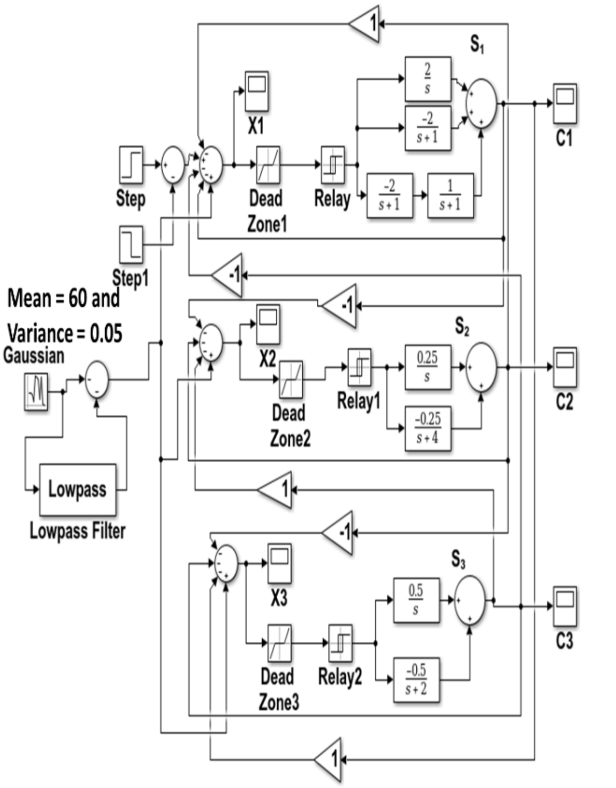

Fig. 16(a): System formulation derived from Figure 9 used to study forced oscillatory response in Example 4 (backlash) subjected to a Gaussian excitation with mean 300 and variance 0.0250.

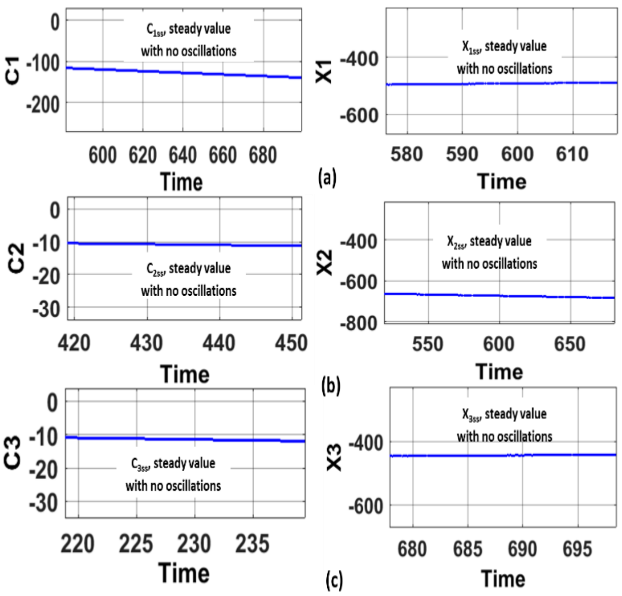

Fig 16(b): Analysis of forced oscillations during signal stabilization under Gaussian excitation (mean 60.0, variance 0.0250) for Example 3 with backlash.

4 Limit cycle suppression in a 3D NL system using PP technique

The PP technique, originally developed for SISO systems [37], can be extended to the suppression of LC or self-sustained oscillations in three dimensional NL systems. The method is based on assigning the closed-loop eigenvalues to preferred locations in the complex plane. This is achieved through the use of an appropriate state-feedback scheme. By selecting suitable eigenvalue positions, the dynamic response of the system can be shaped as desired. To implement this approach, a state-feedback gain matrix K [k_1, k_2, k_3] is designed. The gain values are chosen so that the closed-loop dynamics attain the specified pole configuration. The K can be computed using PP by suitably selecting the desired pole locations, provided that the system satisfies the condition of complete state controllability [49]. In addition, an optimal gain matrix K can be obtained from the Riccati equation. This provides a more systematic and performance-oriented design framework [40, 50].

4.1 Limit cycle suppression in a 3×3 NL system using state feedback-based arbitrary PP

The PP method, implemented via state feedback, is employed to suppress limit cycles by appropriately assigning the closed-loop pole locations. A general multivariable nonlinear (NL) system, in [46], is depicted in Fig. 17(a). This system consists of several interconnected nonlinear elements. Multiple feedback loops are also present and play an important role in governing the overall dynamics. The interactions among these components determine the behaviour and response of the system. For investigation and to show the existence of limit cycles the system is reduced to its autonomous form by setting the external input U=0, thereby eliminating any forcing effects. This simplification isolates the system's intrinsic behavior, allowing the analysis to focus solely on self-sustained oscillations arising from the internal nonlinear interactions. The resulting configuration, shown in Figure 17(b), represents a streamlined system structure. In this form, the interaction between the nonlinearities and feedback paths can be more readily examined for the existence, stability, and characteristics of limit cycles.

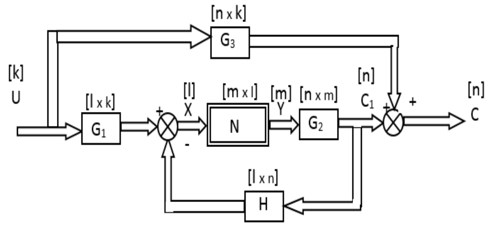

Fig. 17(a): Block diagram of a general multivariable nonlinear system showing interconnected gain matrices (G1, G2, G3), a nonlinear element (N), and a feedback path (H), with input vector [k] and output vector [n].

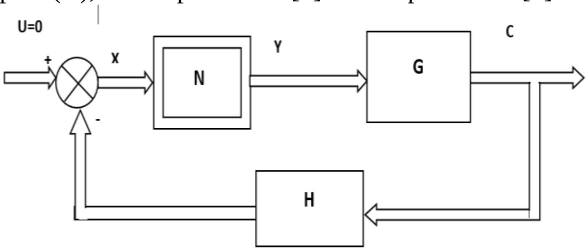

Fig. 17(b): Simplified autonomous form of the nonlinear system (U = 0), showing the nonlinear block (N), linear dynamics (G), and feedback path (H), used to analyze self-sustained oscillations and limit cycles.

By applying first-harmonic linearization to the nonlinear (NL) element, its effect is approximated by an equivalent gain that depends on the amplitude and frequency of the assumed sinusoidal response. This transforms the original nonlinear system into a quasi-linear representation, enabling the use of frequency-domain analysis. As a result, the governing matrix equation for the system in Figure 17(b) is obtained by combining this equivalent gain with the linear dynamics of the blocks and feedback path. The resulting equation relates the oscillation amplitude and frequency through a set of nonlinear algebraic conditions, which must be satisfied simultaneously. Solving these conditions allows the determination of possible limit cycles, including their existence, amplitude, and stability characteristics:

$X = -HC, -HGN(X) = AX$ … (48)

where $C = GN(x)\,X$ and $A = -HGN(X)$

The above equation (48) defines a self-mapping of the state (or harmonic) vector X, meaning that the system dynamics map X back onto itself through the matrix operator A. In this context, a limit cycle corresponds to a non-trivial, steady oscillatory solution that remains invariant under this mapping.

As highlighted in the article [44], two fundamental conditions must be fulfilled for such a solution to occur. First, for any non-zero (non-trivial) vector X, the matrix A must contains an eigenvalue $\lambda=1$. This eigenvalue (=1) condition ensures that the magnitude of X is preserved after one full mapping, indicating neither growth nor decay of the oscillation—an essential requirement for sustained periodic motion.

Second, the eigenvector corresponding to this eigenvalue (=1) must be collinear with the matrix X. This means that the direction of X remains unchanged under the transformation imposed by A, ensuring consistency in the waveform shape and phase across successive cycles. Together, these two conditions guarantee that the system admits a self-consistent oscillatory solution, thereby confirming the existence of a limit cycle along with its associated amplitude and structure.

4.1.1 Application of arbitrary PP for limit cycle suppression in Example 1 involving rectangular hysteresis nonlinearity

The suppression of limit cycles through arbitrary pole placement (PP) is practicable when the system is fully state controllable [49]. This condition ensures that the system states can be influenced through suitable control inputs. The controllability matrix is given by:

$$S = [B \quad AB\; A^2B \ldots\ldots] \qquad \cdots \quad (49)$$

Where,

$$A = \begin{bmatrix} -N_1G_1 & -N_2G_2 & N_3G_3 \\ N_1G_1 & -N_2G_2 & -N_3G_3 \\ -N_1G_1 & N_2G_2 & -N_3G_3 \end{bmatrix}$$

$$B = \begin{bmatrix} 0 \\ 0 \\ 1 \end{bmatrix}$$

$$H = \begin{bmatrix} 1.0 & 1.0 & -1.0 \\ -1.0 & 1.0 & 1.0 \\ 1.0 & -1.0 & 1.0 \end{bmatrix}$$

$$G(\omega) = \begin{bmatrix} G_1(\omega) & 0.0 & 0.0 \\ 0 & G_2(\omega) & 0.0 \\ 0.0 & 0.0 & G_3(\omega) \end{bmatrix}$$

$$N(X) = \begin{bmatrix} N_1(X_1) & 0 & 0 \\ 0 & N_2(X_2) & 0 \\ 0 & 0 & N_3(X_3) \end{bmatrix}$$

$$X = \begin{bmatrix} X_1 \\ X_2 \\ X_3 \end{bmatrix}$$

$$C = \begin{bmatrix} C_1 \\ C_2 \\ C_3 \end{bmatrix}$$

From Table 1(b) for Example 1, LC shows at, $\omega = 0.63$ rad/sec

$X_{m1}= 2.92$, $X_{m2}= X_{m3} =3.26$

$N_1(X_{m1}, \omega) = 0.38$; $N_2(X_{m2}, \omega) = 0.48$, $N_3(X_{m3}, \omega) = 0.48$

$At\ \omega = 0.63, |G_1(j\omega)| = \frac{2}{\sqrt{(\omega-\omega^3)^2+(2\omega^2)^2}} = \frac{2}{\omega(\omega^2+1)} = 2.27$

$|G_2(j\omega)| = \frac{1}{\sqrt{(\omega^2)^2+(4\omega)^2}} = \frac{1}{\omega\sqrt{16+\omega^2}} = 0.39$

$|G_3(j\omega)| = \frac{1}{\omega\sqrt{\omega^2+4}} = 0.75$

$S = \begin{bmatrix} 0 & 0.37 & -0.39 \\ 0 & -0.37 & 0.53 \\ 1 & -0.37 & -0.11 \end{bmatrix}$

Or $|S| = 0.3460 \neq 0$

$\frac{d}{dt}[x(t)] = AX + BU \quad \cdots \quad (50)$

Closed-loop state-space representation of a linear system with state feedback control in Fig. 18.

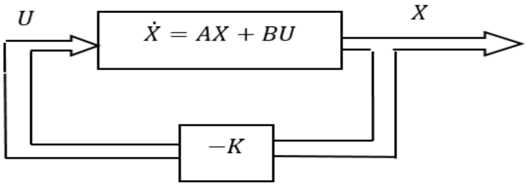

Fig. 18: Closed-loop state-space representation of a linear system with state feedback control u=−Kx, illustrating the dynamics x=Ax+Bu.

The control law : $u = -KX \quad (51)$

Putting K into the Eqn. (65) by Eqn. (66), results in,

$\frac{d}{dt}[x(t)] = (A\text{-}BK)X \quad \cdots \quad (52)$

Upon substituting the values of A, B and K, the Characteristic Equation is given by

$[\![\lambda I - (A - BK)]\!] = 0\ or$

So,

$\begin{bmatrix} (\lambda + N_1G_1) & N_2G_2 & -N_3G_3 \\ -N_1G_1 & (\lambda + N_2G_2) & N_3G_3 \\ N_1G_1 + k_1 & -N_2G_2 - k_2 & \lambda + N_3G_3 + k_3 \end{bmatrix} = 0 \ldots (53)$

$\lambda^3+\lambda^2(1.44+k_3)+\lambda(1.05 + 0.371k_1 + 0.37k_2 + 1.07k_3) + (0.25+0.40k_3 + 0.14k_1) = 0 \cdots \quad (54)$

Let the poles arbitrarily selected as, $\lambda_1 = \lambda_2 = -2.0, \lambda_3 = -3.0$, the characteristic equation results in:

$\lambda^3+7\lambda^2+8\lambda+12=0 \quad \ldots \quad (55)$

$7 = 1.44 + k_3$, whence $k_3 = 4.83 \cdots \quad (56)$

$12 = (0.25 + 0.34k_3 + 0.14k_1) = 0.25+0.86+0.14k_1$, so, $k_1 = 70.92 .. \quad (57)$

$8 = 1.05 + 26.31 + 0.37k_2 + 5.20$, so, $k_2 = -66.24 \quad (58)$

Hence $K = \begin{bmatrix} 0.0 & 0.0 & 0.0 \\ 0.0 & 0.0 & 0.0 \\ k1 & k2 & k3 \end{bmatrix} = \begin{bmatrix} 0.0 & 0.0 & 0.0 \\ 0.0 & 0.0 & 0.0 \\ 70.9 & -66.2 & +4.8 \end{bmatrix} \cdots (59)$

We have,

$A_1 = \begin{bmatrix} -0.88 & -0.19 & 0.37 \\ 0.88 & -0.19 & -0.37 \\ -0.88 - 70.92 & -0.19 + 66.25 & -0.37 - 4.83 \end{bmatrix} \cdots (60)$

The responses obtained from a digital simulation of the autonomous system, presented in Fig. 19.

4.1.2 Application of arbitrary PP via state feedback for limit cycle suppression in Example 2 with backlash NL systems:

From Table 2(b), it is observed that Example 2 (Backlash) exhibits a limit cycle. This occurs at ω = 0.57 rad/sec.

$N_1(X_{m1}, \omega) = 1.290$, $N_2(X_{m2}, \omega) = 1.230$, $N_3(X_{m3}, \omega) = 1.230$

$X_{m1} = 3.0$, $X_{m2} = X_{m3} = 2.3$, $\theta_{L1} = -160.62^o$, $\theta_{L2} = -114.38^o$, $\theta_{L3} = -122.18^o$

At ω = 0.57 rad/sec

$|G_1(j\omega)| = \frac{2}{\sqrt{(\omega-\omega^3)^2+(2\omega^2)^2}} = \frac{2}{\omega(\omega^2+1)} = 2.1565$

$|G_2(j\omega)| = \frac{1}{\sqrt{(\omega^2)^2+(4\omega)^2}} = \frac{1}{\omega\sqrt{16+\omega^2}} = 0.4342$

$|G_3(j\omega)| = \frac{1}{\omega\sqrt{\omega^2+4}} = 0.8436$

The controllability matrix,

$$S = \begin{bmatrix} 0 & 1.03 & -3.41 \\ 0 & -1.03 & 4.51 \\ 1 & -1.03 & -2.36 \end{bmatrix}$$

Or $|S| = 1.151$ which is not equal to zero.

So, arbitrary PP is indeed feasible in this framework, as noted in [49]. For the autonomous case, the closed-loop system structure is illustrated in Figure 18, where state feedback is employed to regulate the system dynamics. The corresponding state-space representation is given by Equation (52), $\frac{d}{dt}[x(t)] = (A\text{-}BK)\ X$. On substitution of A, B and K, the characteristic equation is represented as Equation (53):

$\lambda^3+\lambda^2(N_1G_1+N_2G_2+N_3G_3+k_3)+\lambda(2G_1G_2N_1N_2+2G_1G_3N_1N_3+2N_2N_3G_2G_3+k_1N_3G_3+k_3N_1G_1+k_3N_2G_2+k_2N_3G_3)+(2k_1G_2G_3N_2N_3+4N_1N_2N_3G_1G_2G_3+2k_3G_1G_{2N_1N_2})=0$

For Example 2, the numerical values of $N_1(X_{m1}, \omega)$, $N_2(X_{m2}, \omega)$, and $N_3(X_{m3}, \omega)$, together with $|G_1(j\omega)|$, $|G_2(j\omega)|$ $|G_3(j\omega)|$ are substituted into Equation (53) at ω = 0.57 rad/sec Upon simplification, we obtain the following result:

$\lambda^3+\lambda^2(2.78+0.53+1.03+k_3)+\lambda(2.97+5.77+1.106+1.03k_1+3.31k_3+1.03k_2)+(6.16+2.97k_3+1.10k_1)=0$…(61)

The poles are arbitrarily selected at $\lambda_1=\lambda_2=-3, \lambda_3=-4$, the characteristic equation becomes:

$\lambda^3+10\lambda^2+33\lambda+36=0$ (62)

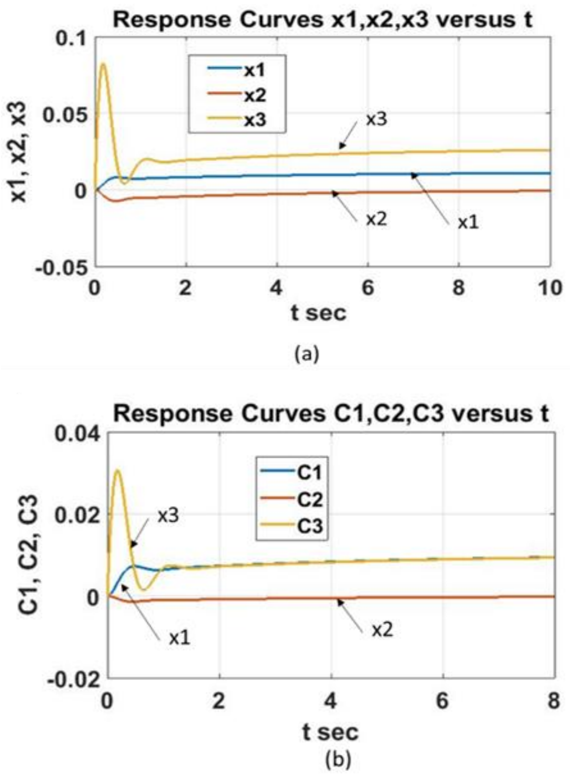

Fig. 19: Limit cycle suppression in Example 1 via arbitrary PP using state feedback.

By equating the coefficients of the corresponding powers of λ, the following relationships are obtained:

$10 = 4.35 + k_3$,

whence $k_3 = 5.64$

$36 = (6.16 + 2.97k_3 + 1.08k_1)$

whence, $k_1 = 12.02$

$$33 = 2.97 + 5.77 + 1.10 + 1.0k_1 + 3.3k_3 + 1.03k_2,$$

whence $k_2 = -7.76$

$$\text{Hence } K = \begin{bmatrix} 0.0 & 0.0 & 0.0 \\ 0.0 & 0.0 & 0.0 \\ k1 & k2 & k3 \end{bmatrix}$$

$$= \begin{bmatrix} 0.0 & 0.0 & 0.0 \\ 0.0 & 0.0 & 0.0 \\ 12.0 & -7.7 & +5.6 \end{bmatrix} \text{... (63)}$$

Eqn. (52) gives, $(A - BK) = A_2$,

$$A_2 = \begin{bmatrix} -2.78 & -0.53 & 1.03 \\ 2.78 & -0.53 & -1.03 \\ -14.80 & 7.76 & -6.68 \end{bmatrix} \text{..... (64)}$$

The responses obtained from a digital simulation of the autonomous system, presented in Fig. 20.

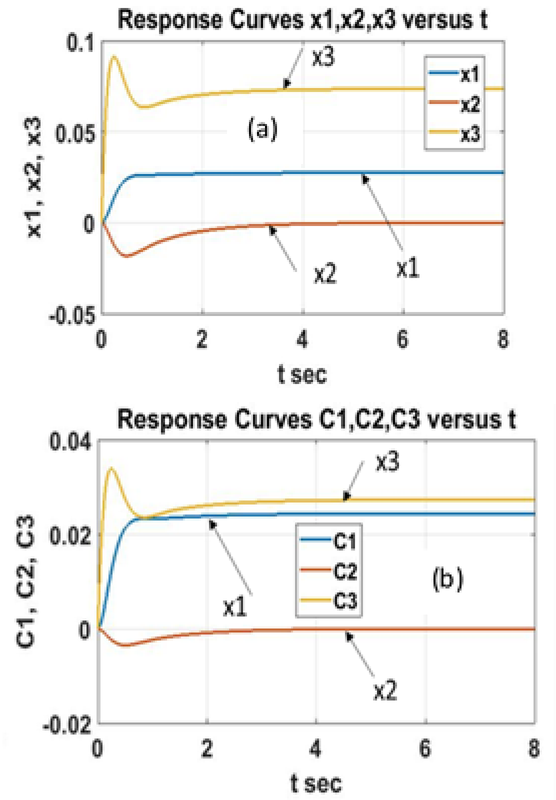

Fig. 20: Limit cycle suppression in Example 4 via arbitrary PP using state feedback

4.2.1 Example 1 (Optimal selection of the feedback gain matrix)

The Riccati equation is expressed as follows:

$$A'F + FA - \frac{FBB'F}{R} + Q = 0 \cdots\cdots (65)$$

And $K = B'F/R$ ··· (66)

It is mentioned $B=\begin{bmatrix} 0 \\ 0 \\ 1 \end{bmatrix}$, $Q = \begin{bmatrix} 1.0 & 0.0 & 0.0 \\ 0.0 & 0.0 & 0.0 \\ 0.0 & 0.0 & 0.0 \end{bmatrix}$, $R = 1.0$,

Considering, the symmetric property of the matrix, F, we have,

$$A'F = \begin{bmatrix} -N_1G_1 & N_1G_1 & -N_1G_1 \\ -N_2G_2 & -N_2G_2 & N_2G_2 \\ N_3G_3 & -N_3G_3 & -N_3G_3 \end{bmatrix}$$

$$\begin{bmatrix} f_{11} & f_{12} & f_{13} \\ f_{21} & f_{22} & f_{23} \\ f_{31} & f_{32} & f_{33} \end{bmatrix} \cdots\cdots (67)$$

$$FA = \begin{bmatrix} f_{11} & f_{12} & f_{13} \\ f_{21} & f_{22} & f_{23} \\ f_{31} & f_{32} & f_{33} \end{bmatrix} \begin{bmatrix} -N_1G_1 & -N_2G_2 & N_3G_3 \\ N_1G_1 & -N_2G_2 & -N_3G_3 \\ -N_1G_1 & N_2G_2 & -N_3G_3 \end{bmatrix} \cdots\cdots (68)$$

$$\frac{FBB'F}{R} = \begin{bmatrix} f_{13}f_{31} & f_{13}f_{32} & f_{13}f_{33} \\ f_{23}f_{31} & f_{23}f_{32} & f_{23}f_{33} \\ f_{33}f_{31} & f_{33}f_{32} & f_{33}f_{33} \end{bmatrix} \quad \ldots. (69)$$

Upon substituting Example 3 values into Eq. 67 results in

$$\begin{bmatrix} (-0.8f_{11}+0.8f_{21}-0.8f_{31}) & (-0.8f_{12}+0.8f_{22}-0.8f_{32}) & (-0.8f_{13}+0.8f_{23}-0.8f_{33}) \\ (-0.1f_{11}-0.1f_{21}+0.1f_{31}) & (-0.1f_{12}-0.1f_{22}+0.1f_{32}) & (-0.1f_{13}-0.1f_{23}+0.1f_{33}) \\ (+0.3f_{11}-0.3f_{21}-0.3f_{31}) & (+0.3f_{12}-0.3f_{22}-0.3f_{32}) & (+0.3f_{13}-0.3f_{23}-0.3f_{33}) \end{bmatrix}$$

$$= A'\,F \quad \cdots\cdots (70)$$

And also upon substituting Example 3 values into Eq. 68 results in:

$$\begin{bmatrix} (-0.8f_{11}+0.8f_{12}-0.8f_{13}) & (-0.1f_{11}-0.1f_{12}+0.1f_{13}) & (+0.3f_{11}-0.3f_{12}-0.3f_{13}) \\ (-0.8f_{21}+0.8f_{22}-0.8f_{23}) & (-0.1f_{21}-0.1f_{22}+0.1f_{23}) & (+0.3f_{21}-0.3f_{22}-0.3f_{23}) \\ (-0.8f_{31}+0.8f_{32}-0.8f_{33}) & (-0.1f_{31}-0.1f_{32}+0.1f_{33}) & (+0.3f_{31}-0.3f_{32}-0.3f_{33}) \end{bmatrix}$$

$$=FA \quad \cdots\cdots (71)$$

Similarly, upon inserting Example 1 values into Eq. (69) - (71) and the Q in Eqn. 65 results in:

$(-1.77f_{11} + 1.77f_{12} - 1.77f_{13} - f_{13}^2 + 1) = 0 \quad \cdots\cdots (72)$

$(-0.881f_{12} - 0.19f_{11} + 0.88f_{22} - 0.19f_{13} + 0.881f_{23} - f_{13}f_{23}) = 0 \quad \cdots\cdots (73)$

$(-1.25f_{13} + 0.37f_{11} + 0.88f_{23} - 0.37f_{12} - 0.88f_{33} - f_{13}f_{33}) = 0 \quad \cdots\cdots (74)$

$(-0.19f_{11} - 1.07f_{12} + 0.88f_{22} + 0.19f_{13} - 0.88f_{23} - f_{13}f_{23}) = 0 \quad \cdots\cdots (75)$

$(-0.38f_{12} - 0.38f_{22} + 0.38f_{23} - f_{23}^2) = 0 \quad \cdots (76)$

$(-0.19f_{13} + 0.37f_{21} - 0.19f_{23} - 0.37f_{22} + 0.19f_{33} - f_{23}f_{33}) = 0 \quad \cdots\cdots (77)$

$0.37f_{11} - 1.25f_{13} + 0.88f_{23} - 0.37f_{12} - 0.86f_{33} - f_{13}f_{33} = 0 \quad \cdots (78)$

$0.37f_{12} - 0.37f_{22} - 0.19f_{13} - 0.56f_{23} + 0.19f_{33} - f_{23}f_{33} = 0 \quad \cdots\cdots (79)$

$0.74f_{13} - 0.74f_{23} - 0.74f_{33} - f_{33}^2 = 0 \cdots (80)$

From Equation (77) and (79), subtraction gives the relation, $f_{23} = f_{32} = 0$

Similarly, subtracting Equation (74) and (78), leads to a trivial solution.

By subtracting Equations (73) and (75), the relation $f_{12} = 2f_{13}$ is obtained. From Equation (76), it follows that $f_{22} = -f_{12} \ \ldots (81)$

Using Equation (80), we obtain

$0.472\,(f_{13} - f_{33}) = f_{33}^2 \ \ldots\ldots\ldots (82)$

From Equation (77), the following expression is derived:

$-\ 0.19f_{13} + 0.37f_{21} - 0.37f_{22} + 0.19f_{33} = 0 \ \ldots\ldots (83)$

Equation (73) gives $f_{11} = -9.73f_{12}$

From Equation (72), the quadratic equation becomes $34.495 - 177\,f_{13} - f_{13}^2 + 1 = 0$, which yields the solutions $f_{13} = 32.75$ or -0.31

Other values are $f_{12} = 0.31$ or -0.06, $f_{22} = -65.50$ or 0.36, $f_{33} = -341.14$ or 0.03

$f_{11} = -637.07$ or -0.59, $f_{23} = 0$

Thus, the complete set of solutions is determined from the above simultaneous relations.

$$F = \begin{bmatrix} f_{11} & f_{12} & f_{13} \\ f_{12} & f_{22} & 0 \\ f_{13} & 0 & f_{33} \end{bmatrix}$$

From Equation (66),

$$K = R^{-1}\,B'F = 1\,[0\ 0\ 1] \begin{bmatrix} f_{11} & f_{12} & f_{13} \\ f_{12} & f_{22} & 0 \\ f_{13} & 0 & f_{33} \end{bmatrix}$$

whence $k_1 = 32.75$ or -0.031, $k_2 = 0$, $k_3 = -341.144$ or 0.032. ----------- (84)

Hence

$$A - BK = A_3 = \begin{bmatrix} -0.88 & -0.19 & 0.37 \\ 0.88 & -0.19 & -0.37 \\ -0.85 & 0.19 & -0.40 \end{bmatrix}$$

The responses of the corresponding C and X are shown in Fig. 21.

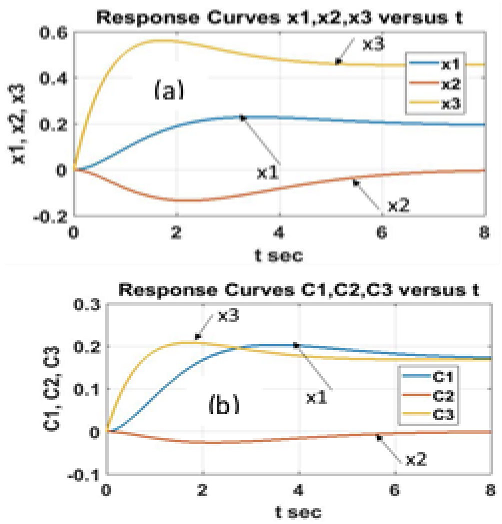

Fig. 21: Responses showing the LC Suppression via State Feedback (Optimal Feedback Gain, Example 1)

4.2.2 Example 2 (Optimal Feedback Gain Matrix Selection)

The Riccati Equation is

$A'F + FA - FBR^{-1}B'F + Q = 0 \ ..\ (65)$

And $K = R^{-1}\,B'F \cdots\cdots (66)$

$$\text{Assuming } A = \begin{bmatrix} -N_1G_1 & -N_2G_2 & N_3G_3 \\ N_1G_1 & -N_2G_2 & -N_3G_3 \\ -N_1G_1 & N_2G_2 & -N_3G_3 \end{bmatrix}$$

$$B = \begin{bmatrix} 0 \\ 0 \\ 1 \end{bmatrix},\ Q = \begin{bmatrix} 1.0 & 0.0 & 0.0 \\ 0.0 & 0.0 & 0.0 \\ 0.0 & 0.0 & 0.0 \end{bmatrix},\ R = 1.0,$$

Let $F = \begin{bmatrix} f_{11} & f_{12} & f_{13} \\ f_{21} & f_{22} & f_{23} \\ f_{31} & f_{32} & f_{33} \end{bmatrix}$ considering F to be symmetric matrix:

$A'F$ =

$$\begin{bmatrix} (-N_1G_1f_{11}+N_1G_1f_{21}-N_1G_1f_{31}) & (-N_1G_1f_{12}+N_1G_1f_{22}-N_1G_1f_{32}) & (-N_1G_1f_{13}+N_1G_1f_{23}-N_1G_1f_{33}) \\ (-N_2G_2f_{11}-N_2G_2f_{21}+N_2G_2f_{31}) & (-N_2G_2f_{12}-N_2G_2f_{22}+N_2G_2f_{32}) & (-N_2G_2f_{13}-N_2G_2f_{23}+N_2G_2f_{33}) \\ (+N_3G_3f_{11}-N_3G_3f_{21}-N_3G_3f_{31}) & (+N_3G_3f_{12}-N_3G_3f_{22}-N_3G_3f_{32}) & (+N_3G_3f_{13}-N_3G_3f_{23}-N_3G_3f_{33}) \end{bmatrix}$$

$\cdots\cdots$ (85)

FA =

$$\begin{bmatrix} (-N_1G_1f_{11}+N_1G_1f_{12}-N_1G_1f_{13}) & (-N_2G_2f_{11}-N_2G_2f_{12}+N_2G_2f_{13}) & (+N_3G_3f_{11}-N_3G_3f_{12}-N_3G_3f_{13}) \\ (-N_1G_1f_{21}+N_1G_1f_{22}-N_1G_1f_{23}) & (-N_2G_2f_{21}-N_2G_2f_{22}+N_2G_2f_{23}) & (+N_3G_3f_{21}-N_3G_3f_{22}-N_3G_3f_{23}) \\ (-N_1G_1f_{31}+N_1G_1f_{32}-N_1G_1f_{33}) & (-N_2G_2f_{31}-N_2G_2f_{32}+N_2G_2f_{33}) & (+N_3G_3f_{31}-N_3G_3f_{32}-N_3G_3f_{33}) \end{bmatrix}$$

$\cdots$ (86)

$$FBR^{-1}B'F = \begin{bmatrix} f_{13}f_{31} & f_{13}f_{32} & f_{13}f_{33} \\ f_{23}f_{31} & f_{23}f_{32} & f_{23}f_{33} \\ f_{33}f_{31} & f_{33}f_{32} & f_{33}f_{33} \end{bmatrix} \cdots (87)$$

Substituting the values of Example 2, where

$A = \begin{bmatrix} -2.782 & -0.534 & 1.038 \\ 2.782 & -0.534 & -1.038 \\ -2.782 & 0.534 & -1.038 \end{bmatrix}$ and Eqn. 85 can be written as

$$\begin{bmatrix} (-2.782f_{11}+2.782f_{12}-2.782f_{13}) & (-2.782f_{12}+2.782f_{22}-2.782f_{23}) & (-2.782f_{13}+2.782f_{23}-2.782f_{33}) \\ (-0.534f_{11}-0.534f_{12}+0.534f_{13}) & (-0.534f_{12}-0.534f_{22}+0.534f_{23}) & (-0.534f_{13}-0.534f_{23}+0.534f_{33}) \\ (1.038f_{11}-1.038f_{12}-1.038f_{13}) & (1.038f_{12}-1.038f_{22}-1.038f_{23}) & (1.038f_{13}-1.038f_{23}-1.038f_{33}) \end{bmatrix}$$

$$= A'\,F \quad \cdots\cdots (88)$$

Upon inserting the values from Example 4, Eqn. (83) is expressed as:

$$\begin{bmatrix} (-2.782f_{11}+2.782f_{12}-2.782f_{13}) & (-0.534f_{11}-0.534f_{12}+0.534f_{13}) & (-1.038f_{11}-1.038f_{12}-1.038f_{13}) \\ (-2.782f_{12}+2.782f_{22}-2.782f_{23}) & (-0.534f_{21}-0.534f_{22}+0.534f_{23}) & (1.038f_{21}-1.038f_{22}-1.038f_{23}) \\ (-2.782f_{13}+2.782f_{23}-2.782f_{33}) & (-0.534f_{13}-0.534f_{23}+0.534f_{33}) & (1.038f_{31}-1.038f_{23}-1.038f_{33}) \end{bmatrix}$$

$$= FA \qquad \cdots\cdots (89)$$

And also upon substituting the values from Eqns. (87) - (89), along with Q, into Riccati Eqn. (65) gives:

$(-5.564f_{11} + 5.564f_{12} - 5.564f_{13} - f_{13}^2 + 1) = 0 \cdots\cdots (90)$

$(-3.316f_{12} - 2.782f_{23} + 2.782f_{22} - 0.534f_{11} + 0.534f_{13} - f_{13}f_{23}) = 0 \quad \cdots (91)$

$(-3.82f_{13} + 2.782 f_{23} - 2.782 f_{33} - 1.038f_{11} - 1.038 f_{12} - f_{13}f_{33}) = 0 \quad \cdots\cdots (92)$

$(-0.534 f_{11} - 3.316f_{12} + 0.534f_{13} + 2.782f_{22} - 2.782f_{23} - f_{13}f_{23}) = 0 \quad \cdots (93)$

$(-1.068f_{12} - 1.068f_{22} + 1.068f_{23} - f_{23}^2) = 0 \quad \cdots (94)$

$(-0.534f_{13} - 1.572f_{23} + 0.534f_{33} + 1.038f_{12} - 1.038f_{22} - f_{23} f_{33}) = 0 \quad \cdots\cdots (95)$

$1.038f_{11} - 1.038f_{12} - 3.82f_{13} + 2.782f_{23} - 2.782f_{33} - f_{13} f_{33} = 0 \quad \cdots\cdots (96)$

$1.038f_{12} - 1.038f_{22} - 1.572f_{23} - 0.534f_{13} + 0.534f_{33} - f_{23} f_{33} = 0 \quad \cdots\cdots (97)$

$2.076f_{13} - 2.076f_{23} - 2.076f_{33} - f_{33}^2 = 0 \cdots (98)$

Subtracting, Equation (91) – Equation (93) = trivial solution and Equation (95) – Equation (97) = trivial solution.

By taking the difference between Equations (97) and (92), it is obtained that, $p_{11} = 0$. By simultaneously solving Eqns. (90)–(98) the values obtained are, $f_{13} = 1.010$, $f_{12} = 1.013$. In a similar manner, solving the set with Eqn. (94) gives $f_{23} = 2.030$ or -0.970 whereas solving the set with Eqn. (98) gives $f_{33} = 0.39$ or -2.11.

From Eqn. (81), $K = R^{-1} B'F$

Or $[k_1 k_2\, k_3] = [(0xf_{11} + 0xf_{12} + 1xf_{13})(\,0xf_{12} + 0xf_{22} + 1xf_{23})(\,0xf_{13} + 0xf_{23} + 1xf_{33})\,]$

Or $[k_1 k_2\, k_3] = [(f_{13})\ \ (f_{23})\ \ (f_{33})\,]$

$= [1.0 \quad 2.0 \text{ or } -0.9 \quad 0.3 \text{ or } -2.1\,]$,

We get, $k_1 = 1.0$, $k_2 = 2.0 \text{ or } -0.9$ and $k_3 = 0.3 \text{ or } -2.1 \quad \cdots\cdots (99)$

So, $A - BK = A_4$ =

$$\begin{bmatrix} -2.78 & -0.53 & 1.03 \\ 2.78 & -0.53 & -1.03 \\ -3.79 & -1.50 \text{ or } 1.50 & -1.43 \text{ or } 1.07 \end{bmatrix} \cdots\cdots (100)$$

For Example 2, the responses

$X = \begin{bmatrix} x_1 \\ x_2 \\ x_3 \end{bmatrix}$ and $C = \begin{bmatrix} C_1 \\ C_2 \\ C_3 \end{bmatrix} = \begin{bmatrix} N_1G_1x_1 \\ N_2G_2x_2 \\ N_3G_3x_3 \end{bmatrix}$ and in the autonomous state, obtained through digital simulation with A_4, These simulated results are presented in Fig. 22.

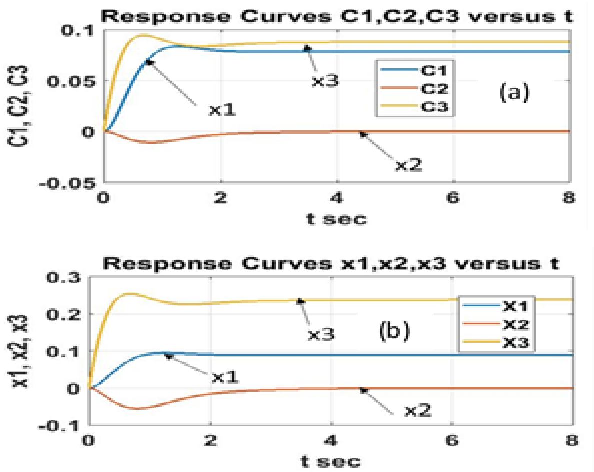

Fig. 22: Response curve showing the LC Suppression using Optimal Feedback Gain, K (Example 2).

5. Conclusion

The presence of limit cycles (LCs) is a clear indication of system instability. Their occurrence can significantly degrade the overall performance of practical control systems. In many engineering applications, persistent oscillations caused by LCs reduce accuracy, efficiency, and reliability. In robotic and automation systems, LCs adversely affect both speed control and position control, leading to poor tracking performance and unwanted vibrations. Similarly, in multi-area power systems, they can create serious difficulties in load–frequency control, thereby reducing the stability and coordination of interconnected areas. Only a limited number of studies have investigated the suppression or complete elimination of LCs in 2×2 systems containing memory-type nonlinearities. The available results therefore remain restricted to lower-order systems.

The present work extends this line of analysis to 3×3 systems. In particular, the study focuses on the quenching of LCs through signal stabilization. It also examines the suppression of LCs by employing a PP approach. The proposed graphical approach offers enhanced insight into the problem owing to its simplicity and ease of implementation. The effectiveness of the method is demonstrated through numerical examples and is further verified using graphical analysis, digital simulations, and implementation in the SIMULINK environment of MATLAB.

The main contributions of this work are as follows:

(1) LCs can be eliminated through signal stabilization using deterministic signals. They can also be suppressed by employing Gaussian signals. This dual approach accounts for uncertainties and helps ensure robust system performance.

(2) LC in 3×3 systems with memory-type nonlinearities can be suppressed using state feedback techniques. This includes arbitrary pole placement under the condition of complete state controllability. It also includes the optimal determination of the feedback gain matrix K through the Riccati equation, representing a novel application not previously reported.

Future work may focus on a comprehensive analysis of synchronization and desynchronization phenomena under both deterministic and stochastic signal stabilization frameworks. Additionally, the proposed approaches can be extended to general n×n systems incorporating both memory and non-memory type Nonlinearities. Furthermore, the development of a fully analytical framework for LC analysis in 3×3 systems with memory-type nonlinearities remains an open research problem. It continues to be an important direction for future.

References:

[1] Gelb, A. (1963) ‘Limit cycles in symmetric multiple NL systems’, *IEEE Trans. Autumn. Control*: AC-8, pp. 177-178.

[2] Gran, R. and Rimer, M. (1965) ‘Stability analysis of systems with multiple Nonlinearities’, *IEEE Trans. Autumn. Control:* 10, pp. 94-97.

[3] Jud, H.G. (1964) ‘Limit cycle determination of parallel linear and non- linear elements’, *IEEE Trans. Autumn. Control*: AC-9, pp. 183-184.

[4] Davison, E.J. and Constantinescu, D. (1971) ‘Describing function technique for multiple NLity in a single feedback system’, *IEEE Trans Autumn. Control:* AC-16, pp. 50-60.

[5] Oldenburger, R. and Nakada, T. (1961) ‘Signal stabilisation of self - oscillating system’, *IRE Trans. Automat Control.* USA, 6, pp: 319-325.

[6] Viswandham, N., and Deekshatulu, B.L. (1966) ‘Stability analysis of NL multivariable systems’, *Int. J. Control*, 5, pp. 369-375.

[7] Gelb, A. and Vader-Velde, W.E. (1968) ‘Multiple-input describing functions and NL system design’, *McGraw- Hill*, New York.

[8] Nikiforuk, P.N., and Wintonyk, B.L.M. (1968) ‘Frequency response analysis of two-dimensional NL symmetrical and non-symmetrical control systems’, *Int. J. Control*, 7, pp.49- 62.

[9] Raju, G.S., and Josselson, R. (1971) ‘Stability of reactor control systems in coupled core reactors’, *IEEE Trans. Nuclear Science*, NS-18, pp. 388-394.

[10] Atherton, D.P. (1975) ‘Non-linear control engineering - Describing function analysis and design’, Van Noslrand Reinhold, London.

[11] Atherton, D.P., and Dorrah, H.T. (1980) ‘A survey on NL oscillations’, *Int. J. Control*, 31. (6), pp. 1041-1105.

[12] Gray, J. O. And Nakhala, N.B. (1981) ‘Prediction of limit cycles in multivariable NL systems’, *Proc. IEE, Part-D*, 128, pp.233-241.

[13] Mees, A.I. (1984) ‘Describing function: Ten years on’, IMA *J. Appl*. Math., 34, 1984 pp. 221-233.

[14] Sebastian, L. (1985) ‘The self-oscillation determination to a category of NL closed loop systems, *IEEE Trans. Autumn. Control*, AC -30, (7), pp. 700-704.

[15] Cook, P.A. (1986) ‘NL dynamical systems’, Prentice-Hall, Englewood ClilTs, NJ.

[16] Chang, H.C., Pan, C.T., Huang, C.L., and Wei, C.C. (1987) ‘A general approach for constructing the limit cycle loci of multiple NLity systems’, *IEEE Trans. Autumn. Control*, AC-32, (9), pp. 845-848.

[17] Parlos, A.G., Henry, A.F., Schweppe, F.C., Gould, L.A., and Lanning, D.D. (1988) ‘NL multivariable control of nuclear power plants based on the

unknown but bounded disturbance model', *IEEE Trans. Autumn.Control*, AC-33, (2), pp.130-134.

[18] Pillai, V.K., and Nelson, H.D. (1988) 'A new algorithm for limit cycle analysis of NL systems', *Trans. ASME, J. Dyn. Syst. Meas. Control*, 110, pp. 272-277.

[19] Genesio, R., and Tesi. (1988) 'A On limit cycles of feedback polynomial systems', *IEEE Trans. Circuits Syst.*, 35, (12), pp. 1523-1528.

[20] Fendrich, O.R. (1992) 'Describing functions and limit cycles', *IEEE Trans. Autom. Control,* AC -31, (4), pp. 486487.

[21] Zhuang, M., and Artherton, D.P. (1994) 'PID controller design lor TITO system', *TEE Proc. Control Theory Appl*. 141, (2), pp. 111-120.

[22] Loh, A.P., and Vasanu, V.V. (1994) 'Necessary conditions for limit cycles in multi loop relay systems', *IEE Proc., Control Theory Appl*., 141, 31, pp. 163-168.

[23] Tesi, A, et al. (1996) 'Harmonic balance analysis of periodic doubling bifurcations with implications for control of NL dynamics', Automatic, 32 (9), 1255, 1271.

[24] Lin, C.H., Han, K.W. (1999) 'Prediction of Limit cycle in NL two input two output control system', '*IEE Proc.-Control Theory Appl*. Vol.146, No.3.

[25] Hori, Y. et al. (1999) 'Slow resonance ratio control for vibration suppression and disturbance rejection in torsional system', *IEEE Trans. Ind. Electron*., vol. 46, (1), pp.162-168.

[26] Nordin, M. and Gutman, P. O. (2002) 'Controlling mechanical systems with backlash- a survey', *Automatica,* vol. 38, (10), pp.1633-1649.

[27] Chidambaram, I.A, and Velusami, S. (2005) 'Decentralized biased controllers for load-frequency control of inter connected power systems considering governor dead band non-linearity, INDICON, Annual *IEEE*, pp.521-525.

[28] Eftekhari, M and Katebi, S. D. (2006) 'Evolutionary Search for Limit Cycle and Controller Design in Multivariable nonlinear systems', *Asian Journal of Control*, , Vol. 8, No. 4, pp. 345 – 358.

[29] Katebi, M, et al. (2009) 'Limit Cycle Prediction Based on Evolutionary Multi objective Formulation', *Hindawi Publishing Corporation,* Mathematical Problems in engineering Volume, Article ID 816707, 17pgs.

[30] Garrido, J, et al. (2009) 'Centralized PID control by Decoupling of a Boiler-Turbine Unit', *Proceedings of the European Control Conference*, Budapest, Hungary, 23-26.

[31] Tsay, T.S. (2011) 'Limit Cycle prediction of NL multivariable feedback control systems with large transportation lags', *Hindawi Publishing corporation journal of control science and Engineering*, article id 169848.

[32] Tsay, T.S. (2011) 'Load Frequency control of interconnected power system with governor backlash Nonlinearities', *Electrical Power and Energy*, vol. 33, pp.1542-1549.

[33] Sujatha, V., Panda, R. C. (2012) 'Relay Feedback Based Time domain modelling of Linear 3-by-3 MIMO System', *American Journal of System Science,* Scientific & Academic Publishing, 1(2), pp. 17-22.

[34] Wang, C, et al. (2015) 'Vibration suppression with shaft torque limitation using explicit MPC-PI switching control in elastic drive systems, *IEEE Trans. Ind. Electron*, vol. 62, (11), pp. 6855-6867.

[35] Yang, M, et al. (2015) 'Suppression of mechanical resonance using torque disturbance observer for two inertia system with backlash', *Proc. IEEE 9th Int. Conf. Power Electron*., ECCE Asia, pp. 1860 - 1866.

[36] Shi, Z, and Zuo, Z. (2015) Back stepping control for gear transmission servo systems with backlash NLity', *IEEE Trans. Autumn. Sci. Eng*., vol. 12, (2), pp. 752-757.

[37] Wang, C., et al. (2017) 'Analysis and suppression of limit cycle oscillation for Transmission System with backlash NLity', *IEEE Transactions on Industrial Electronics,* vol. 62, (12), pp. 9261-9270.

[38] Patra, K. C, and Dakua, B. K. (2018) 'Investigation of limit cycles and signal stabilisation of two dimensional systems with memory type NL elements', *Archives of Control Sciences*, vol. 28, (2), pp. 285-330.

[39] Patra, K. C, Kar, N. (2020) 'Signal Stabilization of Limit cycling two Dimensional Memory Type NL Systems by Gaussian Random Signal', *International Journal of Emerging Trends & Technology in Computer Science,* Vol. 9 Issue 1, pp. 10-17.

[40] Patra, K. C, Kar, N. (2022) 'Suppression Limit cycles in 2 x 2 NL systems with memory type Nonlinearities', *International Journal of Dynamics and Control*, Springer Nature',34, vol.10 Issue 3, pp 721-733.

[41] Iurashev, D., Campa. G., Anishimov V. V. and Cosatto, E. (2017) 'Three step approach for prediction of limit cycles pressure oscillations in combustion chambers of gas turbines', Taylor and Francis, *Combustion Theory and Modelling*, 21(6), 1-28.

[42] Tsay, T.S. (2012) 'Stability Analysis of NL Multivariable feedback Control systems', *WSEAS Transactions on systems,* Volume 11, Issue 4, pp. 140 – 151.

[43] Tripathy, S.C., Hop, G.S. and Malik, O. P. (1982) 'Optimisation of Load-frequency control parameters for power system with read steam turbines and governor dead band NLity', PROC IEE, Ptc. 129(1), 10-16.

[44] Patra, K.C., Patnaik, A. (2023) 'Possibility of Quenching of Limit Cycles in Multivariable NL systems with special attention to 3 x 3 systems', WSEAS Transactions on Systems and Control, Vol. 18.

[45] Oldenburger, R., Sridhar, R., "Signal Stabilization of a Control System with Random Input" *Institute of Electrical Engineers. Part II: Applications and Industry*; Vol.80, Issue 5, 1961, pp 260-268

[46] Patra, K.C., Patnaik, A. (2023) 'Investigation of the Existence of Limit Cycles in Multi Variable NL Systems with Special Attention to 3x3 Systems', *Int. Journal of Applied Mathematics, Computational Science and System Engineering,* Vol. *5,* pp. 93-114.
[47] Sridhar, R., Oldenburger, R. (1962) 'Stability of a NL feedback system in the presence of Gaussian Noise', *Journal of Basic Engineering,* 84, pp. 61-70.
[48] Gibson, J. E., Sridhar, R., (1964) 'The Response of NL closed-loop Systems to Random Inputs', ASME Trans., *Journal of Basic Engineering,* pp. 132-138.
[49] Ogata K, Modern control engineering, 5th Edn. P H I Learning, pp.723-724 and 2012.
[50] Raymond, T, et al. (2002) '*Design of Feedback Control Systems'*, Oxford University Press, 4th edition, pp. 677-678
[51] Singh,Y.P: Some aspects of forced oscillations of non-linear systems (Doctoral dissertation, Ph.D. Thesis, Electrical Engg, IIT Kharagpur, India (1968)

Contribution of Individual Authors to the Creation of a Scientific Article (Ghostwriting Policy)

The authors contributed in the present research, at all stages from the formulation of the problem to the final findings and solution.

Sources of Funding for Research Presented in a Scientific Article or Scientific Article Itself

No funding

Conflict of Interest

The authors have no conflicts of interest to declare that are relevant to the content of this article.